Control of Vacuolar Dynamics and Regulation of Stomatal Aperture by Tonoplast Potassium Uptake

Zaida Andrés[a], Javier Pérez-Hormaeche[a], Eduardo O. Leidi[a], Kathrin Schlücking[b], Leonie Steinhorst[b], Deirdre McLachlan[c], Karin Schumacher[d], Alistair M. Hetherington[c], Jörg Kudla[b], Beatriz Cubero[a], José M. Pardo[a]*

a. Instituto de Recursos Naturales y Agrobiologia de Sevilla, Consejo Superior de Investigaciones Cientificas, Sevilla – 41012, Spain. b. Institut für Biologie und Biotechnologie der Pflanzen, Universität Münster, Schlossplatz 4, 48149 Münster, Germany. c. School of Biological Sciences, University of Bristol, Woodland Road, Bristol BS8 1UG, United Kingdom. d. Centre for Organismal Studies, Universität Heidelberg, Im Neuenheimer Feld 230, 69120 Heidelberg, Germany

Submitted to Proceedings of the National Academy of Sciences of the United States of America

Stomatal movements rely on alterations of guard cell turgor. This requires massive K+ fluxes across the plasma and tonoplast membranes. Although ion influx into the cytosol of guard cells represents only a transit step to the vacuole, the transporters mediating K+ uptake into the vacuole remain to be identified. Here, we report that tonoplast-localized K+/H+ exchangers are pivotal in the vacuolar accumulation of K+ of guard cells and that Arabidopsis nhx1 nhx2 mutant lines are dysfunctional in stomatal regulation. Hypomorphic and complete-loss-of-function double mutants exhibited distinctly impaired stomatal opening and closure responses. Abrogation of K+ accumulation in guard cells correlated with more acidic vacuoles and the disappearance of the highly dynamic remodelling of vacuolar structure associated with stomatal movements. These results establish extensive flux of K+ into vacuoles not only as a physicochemical requisite for stomatal opening, but also as a critical component of the K+ homeostasis that is needed for stomatal closure. Moreover, our data suggest vacuolar K+ fluxes as crucial determinants of vacuolar dynamics that underlie stomatal movements.

Stomata | Vacuole | Potassium | Luminal pH control | Arabidopsis

Introduction

The rapid accumulation and release of K^+ and of organic and inorganic anions by guard cells, controls the opening and closing of stomata and, thereby, gas exchange and transpiration of plants. The intracellular events that underlie stomatal opening start with plasma membrane hyperpolarization caused by the activation of H^+-ATPases, which induces K^+ uptake through voltage-gated inwardly rectifying K^+_{in} channels (1). Potassium uptake is accompanied by the electrophoretic entry of the counterions chloride, nitrate and sulfate, and by the synthesis of malate. These osmolytes, together with sucrose accumulation, increase the turgor in guard cells and thereby drive stomatal opening. Stomatal closure is initiated by activation of the plasma membrane localized chloride and nitrate efflux channels SLAC1 and SLAH3 that are regulated by the SnRK2 protein kinase OST1 and the Ca^{2+}-dependent protein kinases CPK21 and 23 (2, 3). CPK6 also activates SLAC1 and coordinately inhibits rectifying K^+_{in} channels to hinder stomatal opening (4, 5). Sulfate and organic acids exit the guard cell through R-type anion channels. The accompanying reduction in guard cell turgor results in stomatal closure (1).

Despite the established role of plasma membrane transport in guard cell function and stomatal movement, ion influx into the cytosol represents only a transit step to the vacuole since more than 90% of the solutes released from guard cells originate from vacuoles (6). In contrast to the plasma membrane, knowledge of the transport processes occurring in intracellular compartments of guard cells during stomatal movements is less advanced (7). Only recently, AtALMT9 has been shown to act as a malate-induced chloride channel at the tonoplast that is required for stomatal opening (8). Vacuoles govern turgor-driven changes in guard cell volumes by increases and decreases in vacuolar volume during stomatal opening and closure, respectively, by more than 40% (9, 10). Monitoring the dynamic changes in guard cell vacuolar structures revealed an intense remodeling during stomatal movements (11, 12). Pharmacological and genetic approaches indicated that dynamic changes of the vacuole are crucial for achieving the full amplitude of stomatal movement (12-14). However, so far no specific tonoplast transport proteins or processes have been functionally linked to vacuolar dynamics during guard cell movements.

Cation channel activities mediating K^+ release and stomatal closure have been characterized at the tonoplast, including fast vacuolar (FV), slow vacuolar (SV) and K^+-selective vacuolar (VK) cation channels (7, 15). Genetic inactivation of K^+-release channels leads to slower stomatal closure kinetics (7, 16). By contrast, the transporters responsible for the uptake of K^+ into vacuoles against the vacuolar membrane potential that drive the stomatal aperture have remained unknown. We have recently reported that the tonoplast-localized K^+,Na^+/H^+ exchangers NHX1 and NHX2 from Arabidopsis are involved in the accumulation of K^+ into the vacuole of plant cells thereby increasing their osmotic potential and driving the uptake of water that generates the turgor pressure necessary for cell expansion and growth (17). The involvement of K^+,Na^+/H^+ exchangers in the regulation of plant transpiration was also proposed since the *nhx1 nhx2* mutant exhibited enhanced transpirational water loss compared with wild type when subjected to osmotic stress. Here, to resolve whether active K^+ uptake at the tonoplast directly regulates stomatal actitivity by mediating K^+ accumulation in the

Significance

Rapid fluxes of K^+ and other osmolytes in guard cells control the opening and closing of stomata, and thereby gas exchange and transpiration of plants. Despite the well established role of the plasma membrane of guard cells in stomatal function, osmolyte uptake into the cytosol represents only a transient step to the vacuole since more than 90% of the solutes accumulate in these organelles. We show that the tonoplast-localized K^+/H^+ exchangers mediate the vacuolar accumulation of K^+ in guard cells and that activity of these transporters not only controls stomatal opening but also stomatal closure. We also establish vacuolar K^+/H^+ exchange as a critical component involved in vacuolar remodelling and the regulation of vacuolar pH during stomatal movements.

Reserved for Publication Footnotes

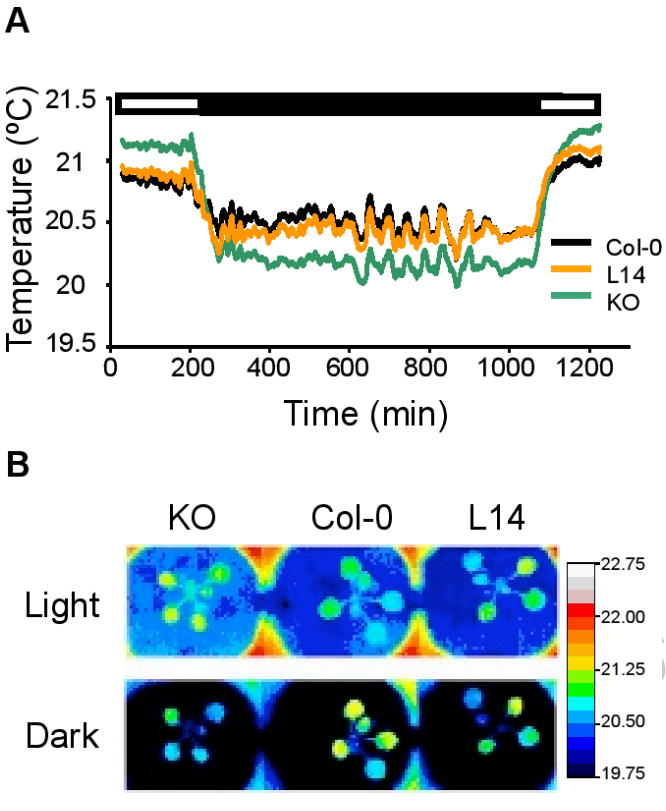

Fig. 1. Thermal imaging suggests that stomata of *nhx1 nhx2* mutants display abnormal behaviour.(A) Data represent the average temperature of two leaves per plant from three different plants of Col-0, L14 and KO lines along light (white box) and dark (black box) periods at one-minute intervals. Error bars have been omitted for clarity; see Table 1 for a statistical analysis. **(B)** Representative pseudocolored infrared images of leaf temperature of Col-0, L14 and KO lines at the light and dark periods.

vacuole of guard cells, we analyzed the stomatal movements of *nhx1 nhx2* double mutant lines using a range of physiological, molecular and imaging-based approaches. Moreover, we have developed a non-invasive, fluorescence ratiometric method to measure vacuolar pH (pHv) in guard cells using the H^+-sensitive and cell-permeant dye Oregon Green and epidermal peels. Our data establish that i) the capacity for K^+ accumulation into guard cell vacuoles is essential for stomatal activity by facilitating not only stomatal aperture but also closure, ii) K^+/H^+ exchange at the guard cell tonoplast mediates the luminal pHv shifts associated to stomata opening, and iii) the dynamic morphological changes that guard cell vacuoles undergo during stomatal movements are brought about by the uptake of K^+ into the vacuole.

Results

Vacuolar K^+ content and morphology of guard cells.

Two Arabidopsis double mutant lines were used in this study, the *nhx1-2 nhx2-1* complete loss-of-function mutant (which we refer to from now onwards as 'KO' line) and line L14 carrying the hypomorphic allele *nhx1-1* together with the null allele *nhx2-1* (17). These knock-out and knock-down mutant lines are useful to learn how varying gene expression levels translate into discernible phenotypical variations. Indeed, the phenotype of the L14 line is similar to, but less severe than that of the KO line due to residual expression of *NHX1*, whereas single *nhx1-2* or *nhx2-1* mutants exhibited negligible growth disturbances (17).

Genes *NHX1* and *NHX2* are preferentially expressed in stomata compared to epidermal and mesophyll cells of leaves (17, 18). As highlighted by SEM images, the stomata of KO plants appeared consistently more open than those of the wild type

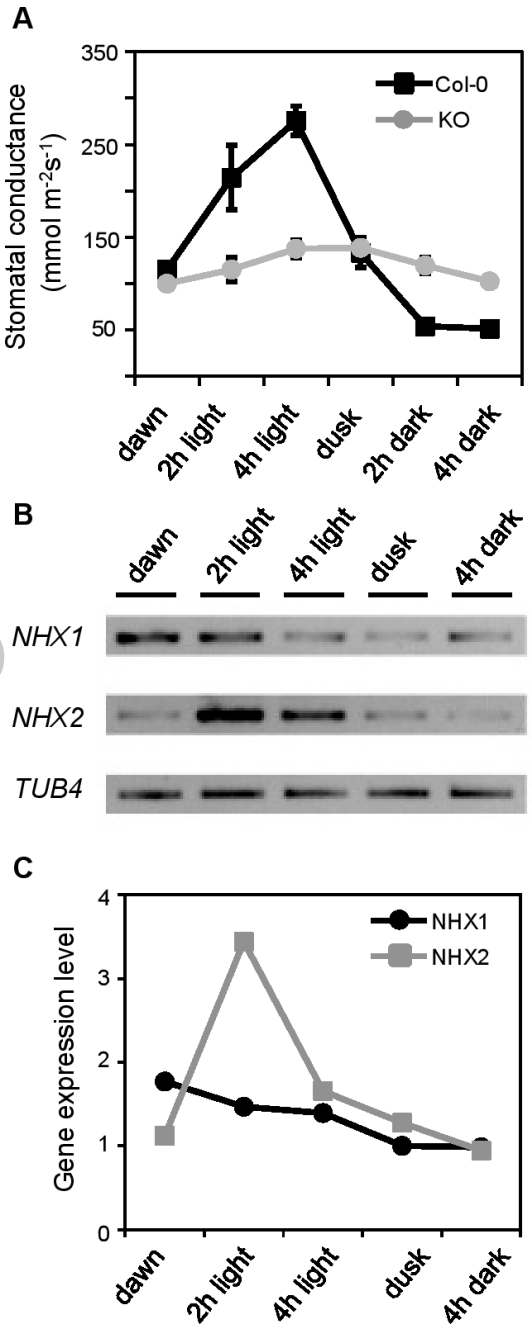

Fig. 2. Diurnal rhythms of stomatal conductance and *NHX* transcript abundance.(A) *In planta* stomatal conductance measurements in Col-0 and KO leaves at different time points of the day/night cycle. Dawn and dusk samples were collected 15 minutes before light was switched on and off, respectively. Data represent mean and SE of 3 plants per line. Mean values were statistically different between wild type and the KO line at $p<0.05$ in pairwise comparison at each time point by the Tukey's HSD test, except for values at the onset of light and at dusk. **(B)** RT-PCR analysis of *NHX1* and *NHX2* mRNA expression levels in whole leaves at different time points of the day/night cycle. The gene *TB4* encoding β-tubulin-4 was used as loading control. **(C)** Relative *NHX1* and *NHX2* gene expression level at different time points of the day/night cycle calculated by densitometry analysis of the bands shown in (B). Each point represents the mean of three different samples per line calculated after normalization to *TB4*. Arbitrary units of gene expression are relative to transcript abundance at 4h of darkness.

(Supplemental Figure 1A) and, with a frequency that varied among samples, guard cells in mutant plants presented aberrant

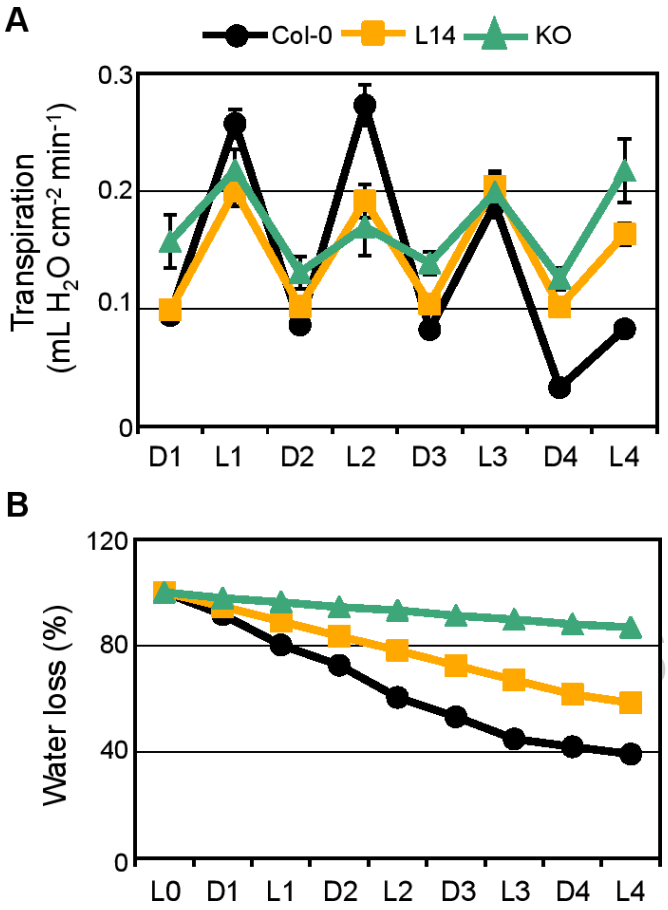

Fig. 3. Reduced water use of *nhx1 nhx2* mutants. (A) Transpiration measurements of Col-0, L14 and KO plants during 4 days of drought stress. Pots were weighed twice daily, at the start of the dark period (D) and at the onset of the light period (L), and transpiration was calculated as the amount of water loss per area unit in each time interval (16 h dark/ 8h light). Data represent the mean and SE of at least 7 plants in individual pots per genotype. **(B)** Percentage of water loss along the drought assay in pots with Col-0, L14 and KO plants. Data represent mean and SE of at least 7 plants per genotype. To quantify the background water evaporation from the soil, identical pots without plants were used as control.

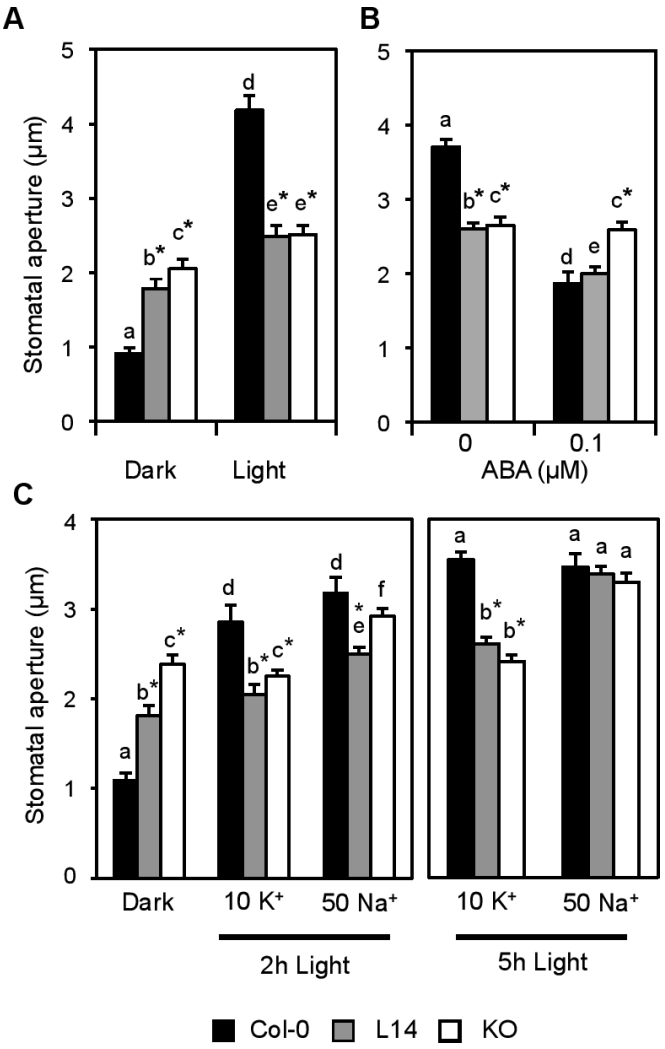

Fig. 4. Defective opening and closure of mutant stomata.(A) Light-induced stomatal opening. **(B)** ABA-induced stomatal closure. **(C)** Light-induced stomatal bioassays in the presence of 10 mM KCl or 50 mM NaCl. Data represent the mean and SE of the absolute values of aperture of at least 40 stomata per line and per treatment. Asterisks indicate statistically significant differences relative to the wild type for each treatment at $p<0.001$ in pairwise comparison by the Tukey's HSD test. Letters indicate statistically significant differences between treatments for each line at $p<0.001$ in pairwise comparison by the Tukey's HSD test.

morphologies and appeared deflated, suggesting that the lack of NHX function compromised the turgor of these guard cells and hindered their swelling capacity. Moreover, the KO mutant line had pavement cells that presented a more heterogeneous cell size distribution than the wild type (Supplemental Figure 1A). To assess whether stomatal lineage and development of guard cells was affected in the null *nhx1 nhx2* plants, epidermal pavement cell and stomatal density were recorded on impressions of the leaf abaxial surface using dental resin. The KO line had significantly less pavement cells than the wild type, but here also the number of stomata per area unit was proportionally lower (Supplemental Figure 1B). Consequently, wild type and mutant lines had similar stomatal indexes, implying that the absence of NHX proteins does not alter the early development of guard cells.

Guard cells of open stomata accumulate large amounts of K^+ in comparison to neighboring epidermal cells (17, 19). The size of the vacuolar K^+ pool was estimated from freeze-fractured leaves exposing the interior of guard cells as described elsewhere (17, 20). Samples were collected 1-2 hours after dawn. The percent of K^+ counts relative to total elemental counts in guard cells of wild type and L14 plants were 1.20 and 0.55, respectively ($p<0.05$ by the LSD method). The K^+ vacuolar content of guard cells in the KO line could not be reliably determined, presumably because of the profoundly altered vacuolar structure in guard cells of the KO plants (see below). These results imply that K^+/H^+ exchange by NHX proteins represents the main pathway for the K^+ uptake into the vacuoles of guard cells.

Infrared thermography reveals altered transpiration rates in nhx1 nhx2 mutants

To investigate how impaired vacuolar K^+ uptake impinged on stomatal function, transpiration rates of whole plants were analyzed by thermal imaging in a light-dark cycle under regular, non-stress growth conditions (21, 22). The leaf temperature of the wild type and of the mutant lines L14 and KO was recorded by obtaining thermal images of 3 to 4-week old plants at 1-min intervals in a 3.5/14/2.5 h light/dark/light cycle. As depicted in Figure 1, during the first light period the leaf temperature in L14 and KO double mutant lines was, on average, significantly elevated compared with wild type (see Supplemental Table S1 for statistical analysis). These results suggested that mutant plants were transpiring less than the wild type, although temperature

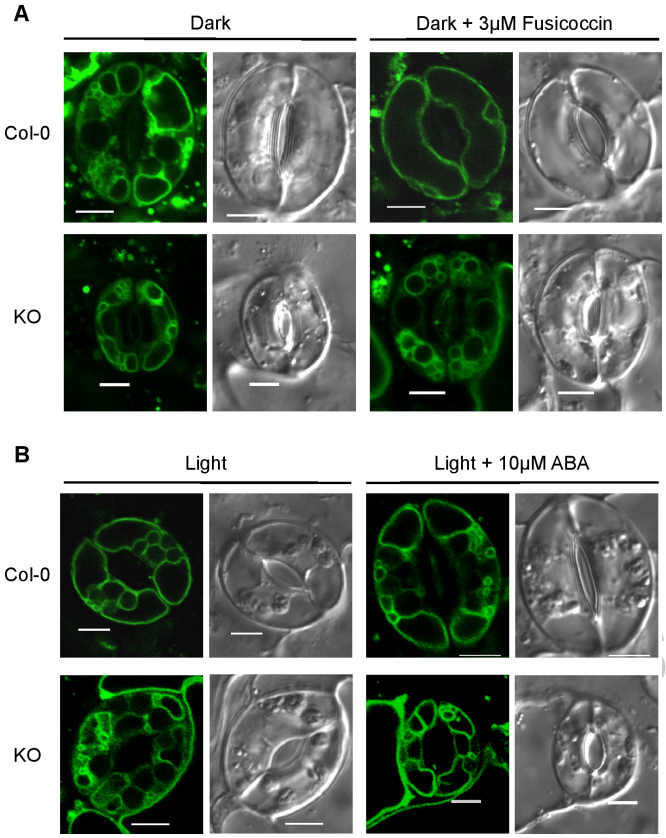

Fig. 5. Vacuolar morphology of guard cells during stomatal movements.(A) Vacuolar structure of Col-0 and KO guard cells visualized with TIP1;1:GFP after dark incubation for 2h (left) and 3 μM fusicoccin treatment for 2h (right). **(B)** Vacuolar structure of Col-0 and KO guard cells visualized with TIP1;1:GFP after illumination for 2h (left) and followed by 10 μM ABA treatment (right). Right and left panels show bright field and GFP images of TIP1;1:GFP, respectively. Scale bar: 5 μm.

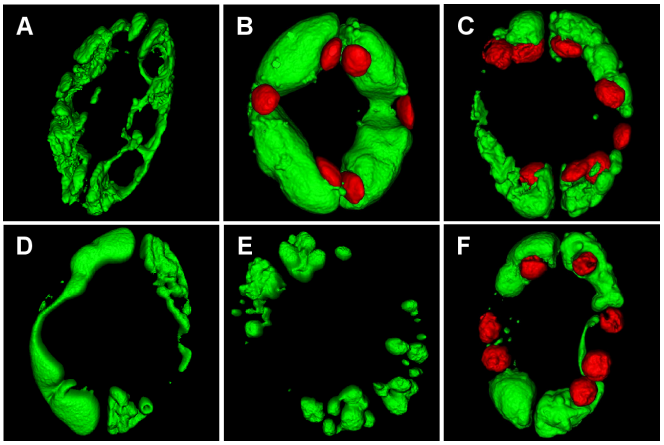

Fig. 6. Three-dimensional projections of vacuolar morphology.(A) Surface rendering of guard cells vacuoles loaded with the BCECF-AM in closed stomata of wild-type plant. **(B)** Vacuolar morphology in open stomata of wild type. Autofluorescence signal of chloroplasts was also captured and shown in red. **(C)** to **(F)** Light-treated stomata of *nhx1 nhx2* mutant plant. Chloroplasts are shown in red (C and F) or have been omitted (D and E).

differences could be explained by dissimilar transpiration rates per area unit, unequal leaf sizes, or a combination of the two. However, the opposite trend was observed during the dark period. The leaves of L14 plants were cooler than wild-type leaves

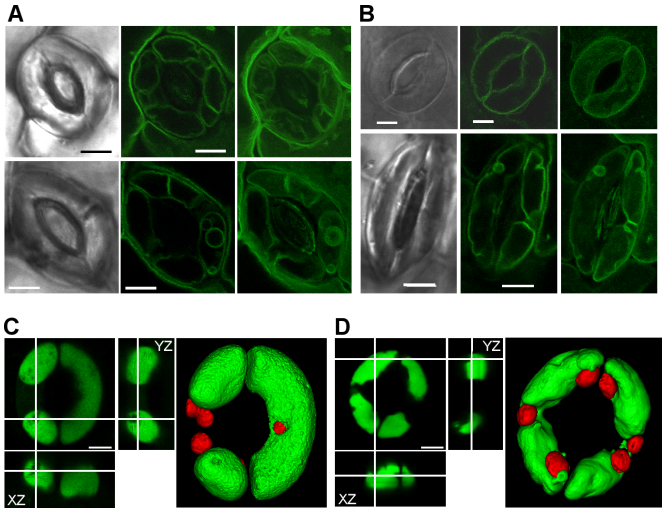

Fig. 7. Alleviation of vacuolar dysfunction by sodium. (A) Vacuolar structure of *nhx1 nhx2* guard cells visualized with TIP1;1:GFP during stomatal opening. Pictures were taken after illumination for 2h in the presence of 10 mM KCl (upper row panels) or 50 mM of NaCl (lower row panels). Left, middle and right column panels show bright field, GFP images, and a 3-D projection of Z-axis images of TIP1;1:GFP, respectively. Scale bar: 5 μm. **(B)** Vacuolar structure in guard cells of the transgenic line expressing NHX2:GFP after illumination for 2h (upper row panels) and after to 2 h of incubation in darkness (lower row panels). The incubation buffer contained 10 mM KCl. Left, middle and right column panels show bright field, GFP images, and a 3-D projection of Z-axis images of NHX2:GFP, respectively. Scale bar: 5 μm. **(C)** Orthogonal views and 3-D surface rendering of Z-axis images of the wild type guard cell vacuoles loaded with 10 μM of BCECF-AM. Pictures were taken after illumination for 3h in the presence of 50 mM of NaCl. Scale bar: 5 μm. **(D)** Orthogonal views and 3-D surface rendering of Z-axis images of the *nhx1 nhx2* guard cell vacuoles loaded with 10 μM of BCECF-AM. Pictures were taken after illumination for 3h in the presence of 50 mM of NaCl. Scale bar: 5 μm.

at the beginning of the dark period (Table S1, periods 2 and 3) but progressively reached wild-type values before the onset of the next light period (Table S1, periods 4 and 5). This result indicated that the hypomorphic mutant line L14 retained the ability to close its stomata at night, albeit more slowly than the wild type. By contrast, leaves of the KO mutant remained cooler than the wild type during the whole dark period (Table S1, periods 2-5), presumably due to the inability of the KO mutant to close its stomata in response to darkness. After the dark/light transition the values observed were similar to those of the first light period (Table S1, period 6).

Disruption of vacuolar K^+ uptake affects the diurnal cycles of stomatal movements

Stomatal movement is one of the many physiological processes controlled by the circadian clock. Opening starts shortly before dawn and closure anticipates dusk to optimize the gas exchange and photosynthetic carbon fixation while preventing undesired water loss (23). To investigate how disruption of vacuolar K^+ uptake influenced stomatal responses to diurnal cycles, stomatal conductance was measured in leaves of single mutants (*nhx1-2*; *nhx2-1*), the double mutant (KO line), and in wild type plants at six different time points in a short-day diurnal period (8h day/16h night). The stomatal conductance of Col-0 leaves increased after dawn and reached a maximum at midday. No significant differences in conductance were found between the wild type and single null mutants *nhx1-2* and *nhx2-1* (Supplemental Figure 2A). By contrast, the stomatal conductance of KO plants exhibited a strongly impaired and delayed response during the day and reached a plateau at dusk, when stomatal conductance in the wild type had already declined (Figure 2A).

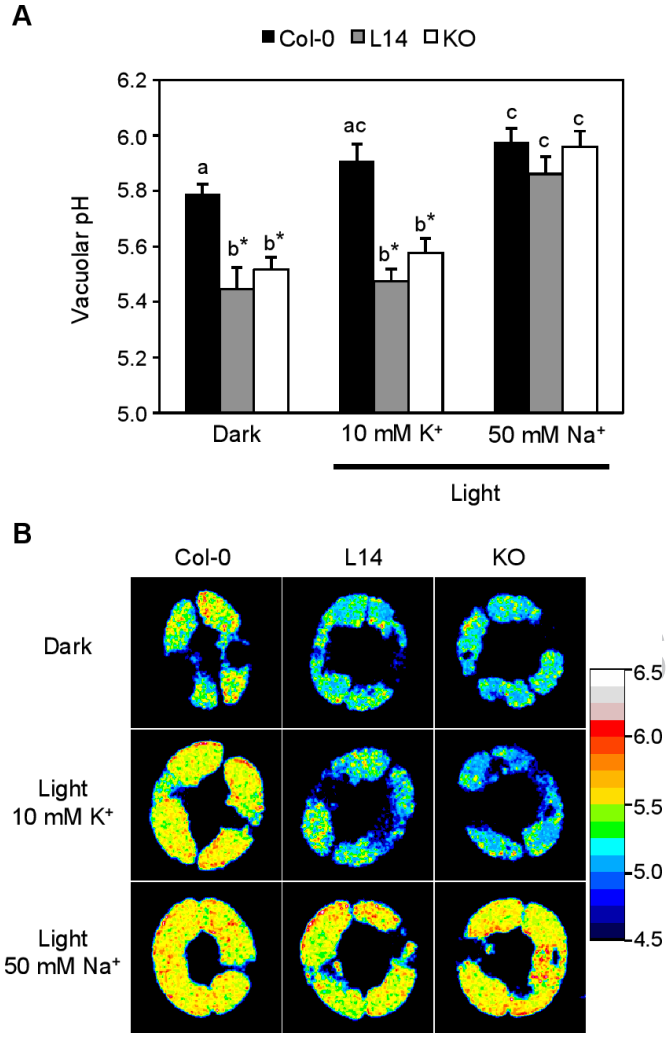

Fig. 8. Acidification of vacuolar pH in mutant guard cells.(A) Vacuolar pH measured after light-induced stomatal opening in the presence of 10 mM KCl or 50 mM NaCl in guard cells loaded with the pH-sensitive dye Oregon Green. Data represent the mean and SE of vacuolar pH values of at least 20 stomata per line and per treatment. Asterisks indicate statistically significant differences relative to the wild type for each treatment at $p<0.001$ in pairwise comparison by the Tukey's HSD test. Letters indicate statistically significant differences between treatments for each line at $p<0.001$ in pairwise comparison by the Tukey's HSD test. **(B)** Representative ratiometric images of wild-type and *nhx1 nhx2* mutant guard cells generated by dividing the emission images obtained in the 488 nm channel by those acquired in the 458 nm channel.

After 2h of darkness the stomatal conductance of the wild type was further reduced, whereas the conductance of the KO mutant slowly declined during the dark period to reach values similar to those found at dawn. These data indicate that not only the amplitude of the stomatal movement was lower in the absence of active K^+ uptake at the tonoplast, but also that stomatal opening and closure in the mutant were more prolonged and delayed compared with the wild type.

Transcripts of *NHX1*, and to a lesser extent *NHX2*, have been reported to undergo circadian regulation in Arabidopsis (24, 25). To corroborate the microarray data, expression of *NHX1* and *NHX2* genes in the course of a light/dark cycle was determined by RT-PCR at five time points of the diurnal cycle in whole leaves (Figure 2B). The abundance of *NHX1* transcript was high before dawn and then declined steadily under daylight (Figure 2C). By contrast, the *NHX2* transcript abundance was low before dawn, climbed to a maximal 3.5-fold upregulation after 2 h of light and then declined steadily to basal levels under darkness. Although the RT-PCR data reflect the transcript abundance in whole leaves and not only guard cells, the diurnal variation of *NHX2* mRNA abundance resembled the dynamics of stomatal conductance (Figure 2A,C). However, the stomatal conductance of the single mutant *nhx2-1* was largely similar to that of the wild type, which could be due to the ca. 40% increase in *NHX1* transcript abundance in the *nhx2-1* mutant under light (Supplememtal Figure 2). No compensatory upregulation of *NHX2* was found in the reciprocal single mutant *nhx1-2*.

Transpiration and soil water consumption of nhx1 nhx2 mutants

Regulation of transpiration is critical for plant water relations and adaptation to water deficit. To study the physiological relevance of stomatal behavior in whole the *nhx1 nhx2* mutant plants, transpiration and water consumption were measured in 7-week old Col-0, L14 and KO plants growing in soil and subjected to water withdrawal. During the first two days without watering the KO mutant showed higher transpiration rates during the dark periods than the Col-0 and L14 lines (Figure 3A). This is in accord with thermography (Figure 1) and stomatal conductance (Figure 2) measurements. By contrast, the two mutant lines exhibited less transpiration than the wild type during the first and second light periods. These results demonstrate that the L14 mutant is more affected in stomatal opening than in stomatal closure whereas the KO mutant is impaired in both processes. The transpiratory oscillations of the wild type changed toward lower transpiration values as the soil dried and plants started to wilt (Supplemental Figure 3A). Wild-type plants first showed wilting symptoms at day 2 after stopping watering, L14 plants after 4 days, and the KO mutant started to shrivel after 2 weeks. The latter survived for more than 25 days. Gravimetric measurements showed that pots with wild type plants had lost 60% of the soil water in 4 days, and that the KO mutant used negligible amounts of water (Figure 3B). Compared to the wild type, mutant lines presented lower K^+ contents in the aerial parts that correlated proportionally with shoot biomass (Supplemental Figure 3B). By contrast, when plants of wild-type and mutant lines were let to compete for soil water, no differences in survival were found (Supplemental Figure 3C). These results indicate that the amount of K^+ that plants were able to collect and store, and not water availability, limited the growth of the *nhx1 nhx2* mutants.

Stomatal movements are severely impaired in nhx1 nhx2 mutant lines.

To better understand guard cell behavior when energetically uphill vacuolar K^+ accumulation is compromised, stomatal responses to light and ABA were investigated on peels of the lower epidermis of wild type and mutant lines. Wild-type stomata were 4.6-fold more open under light than in the dark (Figure 4A). In marked contrast, both dark-induced closure and light-induced stomatal opening were significantly impaired in the L14 and KO lines compared to the wild type. Stomatal apertures in mutant plants kept in the dark were 2-fold that of the wild type, and increased only ~20-30% upon transfer to light. Together, these data indicate that both stomatal closure and stomatal opening processes were affected by mutations *nhx1 nhx2*. An impaired response was also observed when ABA-induced closure of light-opened stomata was tested (Figure 4B). Here, it is noteworthy that while there was a detectable 23% reduction in the stomatal pore in the L14 line after ABA application, the stomata in the KO line were largely unresponsive to the hormonal treatment.

Both ABA and external Ca^{2+} cause increases in cytosolic levels of Ca^{2+} that further relay the signal to downstream responses (1). Because ABA-induced changes in cytosolic pH precede long-term Ca^{2+} transients (26-28) and tonoplast K^+/H^+ exchange might indirectly affect cytosolic pH (29), Ca^{2+}-induced stomatal closure bioassays were conducted to test signal relay

downstream ABA-induced cytosolic alkalinization. In this assay, stomata of L14 plants were again less responsive than the wild type (Supplemental Figure 4A), suggesting that the *nhx1 nhx2* plants arre affected in events that lead to stomata closure further downstream of Ca^{2+} transients.

Despite K^+ being the main cation in guard cell vacuoles in most plant species, Na^+ may substitute for K^+ in stomatal opening, albeit higher concentrations are usually needed to reach the same outcome (30, 31). Accordingly, light-induced stomatal aperture in wild-type plants was sequentially higher with increasing Na^+ concentrations in the incubation buffer, with 50 mM NaCl being required to match the aperture attained with 10 mM of KCl (Supplemental Figure 4B). While mutant plants failed to open their stomata in 10 mM KCl, they were responsive to light in 50 mM NaCl (Figure 4C). Light-induced aperture of mutant stomata in 50 mM NaCl was significantly higher than in 10 mM KCl after 2h, and stomata reached full aperture after 5 h incubation. Wild type and mutants alike failed to close Na^+-opened stomata when treated with 1 μM ABA for 1 h under light. (Supplemental Figure 4C). Previous research has shown that, in Arabidopsis, stomatal closure is impaired after aperture in NaCl because vacuolar Na^+ cannot be readily excreted (32, 33). Together, these results demonstrate that the vacuolar uptake of inorganic cations is a principal component of guard cell expansion and that NHX exchangers play a specific and essential role in the stomatal movements by taking K^+ into the vacuole of guard cells of Arabidopsis. By contrast, they appear to be dispensable for Na^+ accumulation.

Cation uptake is required for accurate regulation of vacuolar dynamics in guard cells.

Guard cell vacuoles undergo dramatic morphological and volume changes that coincide with aperture and closure of stomata (11-13). In fully opened stomata a large vacuole occupies most of the cellular volume whereas in closed stomata the vacuole forms a shrunk and convoluted, but mostly continuous structure. Although the rapid vacuolar dynamics of guard cells must somehow rely on fast changes in water potential, no specific osmolyte flux or transport protein have been experimentally linked to this process. To assess whether vacuolar K^+ uptake affects the vacuolar dynamics in guard cells, transgenic lines of Col-0 and *nhx1 nhx2* knockout mutant expressing the tonoplast intrinsic protein TIP1;1 fused to GFP were created. Epidermal peels were harvested at the end of the night period and stomatal opening was induced chemically by adding 3 μM fusicoccin while keeping the epidermal strips in the dark for 2 hours. Closed stomata from untreated Col-0 epidermal peels exhibited the expected fragmented vacuolar pattern in confocal planes (Figure 5A). Three-dimensional rendering of guard cell vacuoles loaded with the vacuolar dye BCECF-AM revealed however that the vacuole was mostly a continuous structure (Figure 6A). Fusicoccin-treated (Figure 5A) and light-opened stomata (Figure 5B, Figure 6B) appeared completely open in the wild type, and guard cells displayed just one or two large vacuoles occupying the entire cell. The stomatal aperture in the KO line after fusicoccin or light treatments was significantly smaller than the wild type and vacuoles showed the convoluted vacuolar structure indicative of closed stomata (Figure 5A, Figure 6C,D). Remarkably, vacuoles of mutant guard cells were often split into a large number of smaller structures of a vesicular morphology, indicating that vacuolar integrity or the coalescence of endosomal compartments into larger vacuoles was impaired in these plants (Figure 6E). In converse experiments, light-opened stomata showed TIP1;1:GFP fluorescence in a small number of large vacuoles in the wild type (Figure 5B) whereas guard cells of the KO line exhibited distinct or loosely connected compartments (Figure 6F). When wild-type stomata were forced to close by application of ABA, large vacuolar compartments disaggregated and numerous invaginated structures appeared (Figure 5B). By contrast, guard cell vacuoles of the KO mutant remained unaltered and unresponsive to ABA. Together, these findings reveal that vacuolar dynamics during stomatal movements is strictly linked to the function of the NHX exchangers and active K^+ uptake at the tonoplast.

The vacuolar dynamics in guard cells during stomatal movements was also monitored in leaf discs instead of epidermal peels because the stomata remain viable for longer when the pavement epidermal cells are intact, in contrast to epidermal peels where pavement epidermal cells have been disrupted (34, 35). Moreover, stomatal movement was suggested to be mechanistically coupled to leaf turgor and to the water status of neighboring cells (34, 36). Leaf discs of transgenic Col-0 and KO lines expressing the tonoplast marker TIP1;1:GFP were incubated 2 h under light to induce stomatal opening and then mounted in stomatal buffer containing 10 μM of ABA for time-lapse confocal microscopy. Wild-type stomata were completely open prior to ABA application and fluorescence was observed on the vacuolar membrane of a single, large compartment that occupied most of the guard cell volume (Supplemental Figure 5). After 30 minutes, wild-type stomata were completely closed and vacuoles were partitioned into several compartments and invaginations, as observed in confocal planes. By contrast, in the KO mutant the stomatal aperture and the vacuolar morphology did not change at any time before or after ABA application and the vacuolar structures appeared wrinkled and invaginated in smaller compartments (Supplemental Figure 5). Stomatal opening induced with 3 μM of fusicoccin recapitulated, in reverse, the dynamics observed during stomata closure (Supplemental Figure 6). Again, the guard cells of the KO mutant were largely unresponsive to the treatment and the vacuolar structures presented many tonoplast invaginations and smaller compartments. These observations demonstrate that vacuolar dynamics, which coincide with stomatal movements, are severely impaired in plants lacking K^+/H^+ exchangers and establish an essential function of K^+ transport for the accurate regulation of vacuolar dynamics during guard cell movements. These results also suggest that the process of vacuolar remodeling is autonomous in guard cells and not significantly dependent on external effectors originated in neighboring cells since vacuolar dynamics in guard cells were virtually identical in epidermal peels and in leaf discs.

Together, the above data support the conclusion that rapid and drastic changes in vacuolar morphology are crucial mechanisms for guard cell regulation and strongly suggest causality between defective ion uptake at the tonoplast and the absence of vacuolar dynamics. To test if restoration of stomatal aperture in the KO mutant by Na^+ supplementation (Figure 4C) was accompanied with normal vacuolar dynamics, epidermal strips were incubated for 2h under light in buffer containing 10 mM K^+ or 50 mM Na^+. Figure 7A shows that, in contrast to the dysfunctional process driven by K^+, the stomatal aperture of the mutant plant in the presence of Na^+ correlated with the re-establishment of vacuolar dynamics. The structure of Na^+-filled vacuoles was however slightly different from that observed under K^+ supplementation. When Na^+ was used as osmoticum, the structure of the vacuolar compartment in both the wild type and the mutant was more intricate, with the presence of what appeared to be intravacuolar vesicles that were recalcitrant to BCECF-AM loading (Figure 7C). Sodium-loaded vacuoles in the KO line had a wavy surface compared to the wild type (Figure 7D). These findings highlight the importance of cellular turgor adjustment as prerequisite for allowing the dynamic reorganization of vacuolar morphology and volume changes that accompany guard cell movements.

Light-induced stomatal opening and dark-induced closure stomatal bioassays on epidermal peels of the Col-0 line expressing the NHX2 protein fused to GFP revealed that NHX2:GFP fluorescence was mainly observed on the vacuolar membrane

when stomata were fully open (Figure 7B). However, NHX2:GFP fluorescence was observed in several tonoplast invaginations and vesicles in closed stomata, recapitulating what had been observed with the TIP1;1:GFP marker. These results indicate that NHX activity at the tonoplast is directly related to the vacuolar dynamics associated to stomata movements.

Guard cell vacuoles are more acidic in the nhx1 nhx2 mutant than in the wild type.

To determine the vacuolar pH (pHv) of wild-type and mutant guard cells, we established a novel fluorescence ratiometric method using the H^+-sensitive and cell-permeant dye Oregon Green 488 carboxylic acid diacetate in epidermal peels. Oregon Green, which has been used successfully to measure pH in endomembrane compartments in animal cells and fungi (37, 38), loaded specifically the vacuolar lumen of Arabidopsis guard cells (Supplemental Figure 7A). The ratiometric nature of this pH indicator avoids undesired effects caused by unequal loading depending on the compartment size or by differential concentration of the dye at different stages of the vacuolar re-structuration, while the measured fluorescence ratios can be converted to pH values using an in situ calibration curve (Supplemental Figure 7B). Ratiometric fluorescence imaging of guard cell vacuoles in dark-closed stomata showed that the mutant lines had a significantly more acidic vacuolar lumen (Figure 8). Light-induced stomatal opening in the presence of 10 mM KCl elicited a statistically significant alkalinization of wild-type vacuoles by 0.15-0.25 units, depending on the experiment, while the response in mutant vacuoles was curtailed, as was stomatal aperture itself. Notably, substituting NaCl for KCl in the incubation buffer enhanced the aperture of mutant stomata and brought the pHv to wild-type values. The results indicate that K^+/H^+ exchange by NHX proteins is essential to maintain the correct pH in guard cell vacuoles and that restoration of stomatal opening by NaCl in the mutant correlates with the re-establisment of wild-type pHv values.

Discussion

Stomatal movements rely on turgor and volume changes in the guard cells. The main solutes involved in guard cell osmoregulation are K^+ and sucrose, and accompanying anions (chloride, nitrate, sulfate and malate), depending on the environmental conditions and the time of the day (7, 39, 40). Due to the high mobility of K^+ and because it is an energetically cheap solute, guard cells accumulate K^+ salts in large amounts, mainly in the vacuole, to open the stomata (41). Accumulation of K^+ into the vacuole against the electrochemical gradient is necessary to generate sufficient turgor for stomatal opening, and this uphill K^+ transport has to be mediated by secondary active carriers (34, 42). Here, we show that this critical function is carried out by vacuolar K^+/H^+ antiporters. Light- and fusicoccin-induced stomatal opening was severely impaired in *nhx1 nhx2* mutants in the presence of KCl (Figures 4 and 5) and fully restored by NaCl (Figure 4). The restoration of vacuolar dynamics and wild-type pHv by incubation in NaCl strongly indicates that stomatal movement defects are not due to a general mechanical failure of mutant guard cells, but are linked to a process that is dependent on the ability to accumulate alkali cations in the vacuole. Mutant plants exhibited reduced stomatal conductance (Figure 2) and transpiration (Figure 3) compared with the wild type during the light photoperiod when the stomata open. The 50% reduction in maximal transpiration rate of the KO mutant relative to the wild type (Figure 2) was twice as large as the reduction in stomatal density (Supplemental Figure 1), indicating that the KO mutant had not only fewer stomata per leaf area unit but also that their aperture was compromised. Thermal imaging and stomatal bioassays showed that the leaky mutant presented a less severe stomatal dysfunction than the null double mutant. Presumably the activity of NHX1 remaining in the hypomorphic *nhx1-1* allele allowed some accumulation of K^+ into the vacuoles, thereby allowing stomatal opening and closure. This is consistent with the relative K^+ contents of these mutant lines (Supplemental Figure 3B). It is worth noting that the curtailed and delayed responses of stomata in the null mutant in daily cycles led to the counterintuitive finding that mutant plants survived longer under water deprivation because the plants were not only smaller but they also transpired less per leaf area unit during the day, thus consuming less soil water. Water loss at night in the mutant was greater compared to the wild type, but this was apparently compensated by diurnal water savings (Figure 3). However, when wild type and mutant plants shared the soil and competed for water, the mutant plants had no selective advantage and wilted at the same rate than the wild type (Supplemental Figure 3C).

Although full stomatal opening was impaired in *nhx1 nhx2* mutant plants, their stomata retained a limited response to diurnal cycles (Figure 2 and 3). The lowest limit for vacuolar K^+ concentration appears to be 10 to 20 mM, which is thought to reflect equilibrium with the cytosol at a maximum trans-tonoplast voltage of 40 to 60 mV (42, 43). Systems modeling of guard cell transport and volume control suggested that bidirectional K^+ flux (i.e., including K^+ uptake for stomata opening) across the tonoplast was largely mediated by the TPK channel, with only minor contributions of the FV and TPC channels (44). Our data indicate however that tonoplast K^+ channels facilitated minimal K^+ uptake into the vacuole of guard cells, that was by itself insufficient to promote full stomatal aperture in the *nhx1 nhx2* mutants. The more acidic pHv in the mutant relative to the wild type is also in agreement with a substantial K^+/H^+ exchange by NHX proteins at the tonoplast thereby recycling H^+ toward the cytosol. Sucrose and other organic osmolytes also accumulate in the vacuole of guard cells during stomatal opening and could explain the limited stomatal opening capacity observed in KO plants. However, the photosynthesis-dependent accumulation of sucrose mainly occurs during the late light period, when K^+ concentrations have already decreased (39, 40). Prior K^+ accumulation to drive the rapid stomatal opening at dawn is an essential prerequisite for the sucrose-dominated phase, indicating that in the afternoon sucrose replaces K^+ for turgor maintenance instead of just enhancing stomatal opening. Our results are consistent with the two-phase osmoregulation in guard cells of Arabidopsis (19). Stomatal conductance increased sharply in wild-type plants but it progressed at a slow pace in the KO mutant, reaching its maximum by the end of the day presumably due to the comparatively slow accumulation of photosynthesis-dependent organic solutes (Figure 2). The slow closure at night likely reflects the release of the less mobile sucrose in the mutant. Therefore, NHX proteins are directly involved in the K^+ accumulation that drives the rapid stomatal opening that takes place at the start of the light period, but their lack also irreparably affects the succeeding sugar-dependent phase.

Unexpectedly, stomata closure was also affected in *nhx1 nhx2* mutants. Stomatal closure is largely dependent on the activation of ion efflux channels in the vacuolar and plasma membranes (7). Arabidopsis plants lacking the vacuolar K^+-release channel TPK1 display slower stomatal closure but normal opening kinetics (16), whereas inactivation of the plasma membrane anion release channel SLAC1 impaired both stomatal closure and opening (45, 46). The impairment of *slac1* mutant on stomatal opening is due the reduction of inward K^+ channel activity and enhancement of outward K^+ currents by a compensatory feedback control that is triggered by the increase of cytosolic Ca^{2+} and of 0.2 pH_{cyt} units in the *slac1* mutant (45, 46). Impairment of stomatal closure in the *nhx1 nhx2* mutants suggests that the requirement for active K^+ uptake at the tonoplast represents not simply the end point in the process of stomatal opening. Instead, this finding implies that

the K^+ status of guard cells feeds-back on the closure of stomata by a yet unknown mechanism. Mechanistically, this inhibition of stomatal closure might be mediated the combination of the 2-fold reduction in vacuolar K^+ content (this work) and of enhanced K^+ cytosolic accumulation in the *nhx1 nhx2* mutant (17) that together could compromise depolarization of the tonoplast by vacuolar K^+ efflux prior to stomatal closure. A similar mechanism has been suggested for the slightly impaired stomatal closure observed in Arabidopsis lacking the vacuolar anion/H^+ exchanger AtCLCc (34, 47). Notably, the vacuolar chloride-uptake channel AtALMT9 is required for fast and complete stomatal opening but has no effect on stomata closure (8), in contrast to defective K^+ uptake.

Guard cell vacuoles undergo remarkable morphological changes that contribute to stomatal opening and closure movements (13). Vacuole remodeling allows a swift and dramatic reduction in cell volume for stomatal closure while maintaining the total membrane surface area that is essential for rapid stomatal reopening (11, 13, 48). Here, we have investigated the role of vacuolar K^+ uptake in guard cell vacuolar dynamics during stomatal movements using Arabidopsis Col-0 and null *nhx1 nhx2* plants expressing TIP1;1:GFP fusion. Three-dimensional reconstruction of wild-type vacuoles revealed a single or a few main continuous vacuolar compartments that appeared deflated and convoluted in closed stomata, and that expanded to form a readily detectable single vacuole in open stomata. Compared with control plants, null mutants were unable to merge and expand the smaller vacuolar compartments resulting in the failure of stomatal opening. Under stomata-closing conditions, guard cells of the KO plants contained several compartments that appeared to be smaller, and tonoplast invaginations and a wavy vacuolar surface that changed little over the time course of the treatment. This lack of vacuolar motility correlated with the inability of the null mutant to fully open and close the stomata. One of the mechanisms proposed for vacuolar expansion in guard cells consists of passive fusion of endosomes due to physical contact between neighboring vesicles that increase their size by accumulating ions and water (13). This may explain why the lack of K^+ uptake at the tonoplast affected the vacuolar morphology. The null mutant could not accumulate enough K^+ and the subsequent water entry into the vesicles was impaired. Consequently, small vacuoles could not enlarge and fuse to each other. This conclusion is supported by the restoration of vacuolar dynamics and stomatal opening in the KO mutant when Na^+ replaced K^+ as the main osmoticum in the assay. Another not mutually exclusive mechanism could be provided by vesicle fusion caused by pH changes in the lumen of the vesicles and in their surrounding cytoplasm. In *Saccharomyces cerevisiae*, the endosomal Na^+,K^+/H^+ antiporter homologous to the Arabidopsis NHX1 and NHX2 proteins regulates vesicle fusion by controlling the luminal pH through its ion exchange activity (49). The K^+/H^+ antiporter activity of the NHX proteins coupled to V-ATPase and V-PPases activities would drive these pH changes in plants. The vacuolar lumen is more acidic in guard cells of *nhx1 nhx2* null mutants than in wild type (Figure 8) whereas the opposite was found in Arabidopsis mutants with defective vacuolar proton pumps VHA and VHP that had delayed ABA-induced stomatal closure (12). The lack of tonoplast K^+/H^+ exchangers could therefore impair stomatal function by affecting pH-dependent processes in addition to their contribution to the purely physicochemical component of turgor-driven stomatal movements. Acidification of the vacuolar lumen inhibits the opening of the tonoplast efflux channel TPC1 (50), which may contribute further to the inhibition of stomatal closure in *nhx1 nhx2* plants. Taken together, these data suggest a two-tier contribution of K^+/H^+ exchangers in the stomatal movements in Arabidopsis. Ensuing the generation of proton gradients by the activation of the plasma membrane and tonoplast H^+-pumps, the NHX proteins couple two simultaneous processes: the alkalinization of the endosomal compartments to initiate vacuolar fusion which results in an increase of vacuolar surface area and volume, and the accumulation of osmotically active K^+ with the subsequent entry of water and increase of cell turgor.

In summary, our results establish that the large uptake flux of K^+ at the tonoplast of guard cells is not only a physicochemical requisite for stomatal opening, but also a critical step to sustain the K^+ homeostasis that is needed for stomatal closure. Moreover, this study reveals that ion transport activity by NHX proteins represents the basis for the intense remodeling of the vacuoles and associated endosomes that take place concurrently with stomatal movements.

Materials and Methods

Plant material and growth conditions

Single and double mutant lines of *Arabidopsis thaliana* carrying alelles *nhx1-1*, *nhx1-2* and *nhx2-1* have been described elsewhere (17). Plants of were grown on soil in a Sanyo MLR-351 plant growth chamber under the day/night regime: 23/19ºC, 60-70% relative humidity, 8/16 h illumination, and 250 µmol m^{-2} s^{-1} photosynthetically active radiation (PAR).

Gene constructs for plant transformation

NHX2:GFP and TIP1;1:GFP translational fusions were created using the GFPmut1 variant with enhanced fluorescence and optimized for translation in eukaryotic cells (51), and the cDNAs of the *NHX2* (At3g05030) and *TIP1;1* (At2g36830) genes. Detailed information on primers, plasmid constructs, and production of transgenic lines is given in Supplemental Methods.

Thermal imaging

Thermal images of 3-4 week-old plants were obtained using a ThermaCam SC5000 infrared camera (Inframetrics, FLIR Systems) placed in a chamber with constant humidity (70%), temperature (21ºC) and light intensity (90 µmol m^{-2} s^{-1}). Images were obtained at 1-minute intervals in a 3,5/14/2,5h light/dark/light cycle. Leaf temperature was calculated as the average temperature of the pixels contained into a standard area drawn on leaves using the FLIR Altair software. Data represent the temperature moving average of two leaves per plant from three different plants per line. Representative images were saved as 8-bit TIFF files and treated with the analysis program ImageJ (National Institutes of Health, USA; http://rsbweb.nih.gov/ij/).

Stomatal conductance measurements

Leaf gas exchange was determined using the steady state porometer LI-1600 (LI-COR). Stomatal conductance rate (mmol of water m^{-2} s^{-1}) was measured in 6 to 7-week-old plants. Measurements were recorded at six different points of the day: light onset, 2h and 4h of light, dusk, 2h and 4h after darkness. A total of 3 measurements for each genotype (3 plants per line) were recorded and mean and standard error calculated.

Stomatal bioassays

Light-induced stomatal opening bioassays were done on leaves of 4-6 week-old-plants. Strips of leaf abaxial epidermis were harvested at the end of the night period and incubated for 2 h in darkness in stomatal incubation buffer containing 10 mM MES-KOH, 10 mM KCl, 50 µM $CaCl_2$, pH 6.5 and then for 2 h under light (250 µmol m^{-2} s^{-1}) at 22°C (16, 50, 52). In Na^+-supported stomatal opening bioassays KCl was replaced for NaCl (30, 50 or 75 mM) in the stomatal incubation buffer. Images were captured with a CCD digital camera connected to a Zeiss Axioskop microscope and stomatal apertures were measured with the AxioVision software (Zeiss). For fusicoccin-induced stomatal opening experiments, abaxial epidermal peels were pre-incubated for 2 h in the dark before treatment with 3 µM fusicoccin from *Fusicoccum amygdali* (Sigma) for another 2 h in darkness (11). For Ca^{2+}- and ABA-induced stomatal closure experiments, epidermal strips were pre-incubated for 2 h under light. Then, 2 mM and 5 mM of $CaCl_2$ or 0.1 µM of ABA were added, and stomatal closure was measured 2 h after treatment. Four different plants were used for each experiment, taking one leaf of each plant per treatment. Stomatal apertures were determined by measuring the inner width of the stomatal pore from captured photographs of a minimum of 40 stomata per line and condition. Stomatal bioassays were performed three times and measured as blind experiments.

Confocal microscopy of vacuolar dynamics

To monitor the vacuolar dynamics in guard cells during stomatal movements, bioassays were performed using the transgenic lines expressing TIP1;1:GFP and NHX2:GFP proteins as described above but using 10 µM of ABA to promote stomatal closure and 3 µM of fusicoccin to stimulate stomatal opening. Images were taken with a FluoView FV1000 Confocal Microscope (Olympus) using a 488-nm Ar/ArKr laser and a 60X objective with emission signals being collected at 525 ± 50 nm. Images were analyzed with the FluoView 2.1 software (Olympus). For time-lapse experiments, leaf discs were pre-incubated in stomatal incubation buffer for 2h in the dark or under light, to close and open the stomata respectively. Then, microscope samples were prepared adding the stimulus (3 µM of fusicoccin to open the closed stomata or 10 µM of ABA to close the open stomata) and immediately images

of single stomata at different times were taken. Interval times were the same for wild-type and mutant lines. Three-dimensional renderings of guard cells vacuoles loaded with BCECF-AM were done as described (53, 54) using the ImageJ plugin 3-D Viewer.

Vacuolar pH measurement

Guard cell-vacuolar pH of epidermal peels was determined using the fluorescent cell-permeant dye Oregon Green 488 carboxylic acid diacetate (OG-CADA, Molecular Probes). Loading of the dye was performed by floating the epidermal peels in liquid media containing 1 mM KCl, 10 mM MES-KOH (pH 5.8), and 50 μM $CaCl_2$ in the presence of 10 μM OG-CADA and 0.01% Pluronic F-127 (Molecular Probes). The low-toxicity dispersing agent Pluronic facilitated cell loading of the membrane-permeant ester OG-CADA and OG was subsequently accumulated into vacuoles upon hydrolysis of the esterified groups by intracellular esterases (38) with little or no fluorescence in the cytosol (Supplemental Figure 7A). After 90 min of staining at 22 °C in darkness, the epidermal peels were washed twice for 10 min in dye-free buffer. Then, the epidermal peels were incubated for 3 h, and exposed to different stimuli, in 10 mM KCl, 10 mM Mes-KOH (pH 6.5), and 50 μM $CaCl_2$. Fluorescence microscopy was performed on a Leica SP5II confocal laser scanning microscope equipped with an inverted DMI6000 microscope stand and a HCX PL APO x63 water immersion objective. The fluorophore was excited at 488 and 458 nm, respectively, and the emission was detected between 510 and 550 nm. To obtain the ratio values the images were processed as described (54). The ratio was then used to calculate the pH on the basis of a calibration curve (Supplemental Figure 7B). In situ calibration of OG-CADA was performed in epidermal peels, which were loaded with the dye as mentioned above. Then, epidermal peels were incubated for 90 min in liquid media containing 10 mM KCl, 10 mM MES-KOH (pH 6.5). Twenty minutes before measurements the peels were incubated in pH equilibration buffers containing 50 mM citrate buffer-BTP (pH 4.5-5.0) or 50 mM MES-BTP (pH 5.5 – 6.5) and 50 mM ammonium acetate. Ratio values were plotted against the pH and the calibration curves were generated using a sigmoidal Boltzmann fit.

Drought assay and transpiration measurements

Seven-week old Col-0, L14 and KO plants were subjected to the same watering regime during the plant growth phase and pots were covered with plastic film to avoid water evaporation from the soil. Prior to initiate the drought phase, pots were well watered until the soil reached the field capacity and the surplus water drained away. The start of the drought tolerance assay coincided with the beginning of the dark period. Pots were weighed at dusk and at the light onset during four consecutive days and transpiration (mL H_2O cm^{-2} min^{-1}) was calculated. At least 7 plants per line were used and their foliar area was calculated with the AxioVision software (Zeiss) from images of their rosettes to determine the transpiration rate per area unit. Five days after stress imposition plants were sampled (3-4 plants per line) and the dry weight and K^+ and water contents were determined as described (20). Images of the plants were taken at different time points until all plants died.

Acknowledgements.

We are indebted to Imelda Mendoza, Maria A. Parrado and Ana I. Ferrer for technical assistance, to Melanie Krebs and Falco Krüger for assistance with vacuolar dye loading and 3-D image rendering, and to Francisco J. Quintero and Irene Villalta for helpful discussions. This work was supported by grants BIO2009-08641 and BFU2012-35060 from Ministerio de Economia y Competitividad (MINECO, cofinanced by the European Regional Development Fund) to J.M.P., and by grants Ku931/7-1, SFB629 and FOR964 from the Deutsche Forschungsgemeinschaft (DFG) to J.K., and FOR1061 (DFG) to K.S. AMH wishes to acknowledge support from the Biotechnology and Biological Sciences Research Council of the UK. Z.A. was supported by the Junta de Ampliacion de Estudios Fellowship Program of Consejo Superior de Investigaciones Cientificas. The funders had no role in study design, data collection and analysis, decision to publish, or preparation of the manuscript.

Author Contributions Z.A., J.P-H., E.O.L., K.S., L.S., D.M., and B.C. performed the research. Z.A., E.O.L., B.C., K.S., A.M.H., J.K, and J.M.P. designed the research. Z.A., B.C., A.M.H., J.K. and J.M.P. wrote the article. **Conflict of Interest** Authors declare no financial or personal interests that could be construed to have influenced this work. **Supporting Information** This article contains supporting information (Supplementary text and figures).

1. Kim TH, Bohmer M, Hu H, Nishimura N, Schroeder JI (2010) Guard cell signal transduction network: advances in understanding abscisic acid, CO2, and Ca2+ signaling. *Annual Review of Plant Biology* 61:561-591.
2. Geiger D, *et al.* (2009) Activity of guard cell anion channel SLAC1 is controlled by drought-stress signaling kinase-phosphatase pair. *Proc Natl Acad Sci U S A* 106:21425-21430.
3. Geiger D, *et al.* (2010) Guard cell anion channel SLAC1 is regulated by CDPK protein kinases with distinct Ca2+ affinities. *Proc Natl Acad Sci U S A* 107:8023-8028.
4. Brandt B, *et al.* (2012) Reconstitution of abscisic acid activation of SLAC1 anion channel by CPK6 and OST1 kinases and branched ABI1 PP2C phosphatase action. *Proc Natl Acad Sci U S A* 109:10593-10598.
5. Ye W, *et al.* (2013) Calcium-dependent protein kinase CPK6 positively functions in induction by yeast elicitor of stomatal closure and inhibition by yeast elicitor of light-induced stomatal opening in Arabidopsis. *Plant Physiol* 163:591-599.
6. MacRobbie EA (1998) Signal transduction and ion channels in guard cells. *Philos Trans R Soc Lond B Biol Sci* 353:1475-1488.
7. Hedrich R (2012) Ion channels in plants. *Physiological Reviews* 92:1777-1811.
8. De Angeli A, Zhang J, Meyer S, Martinoia E (2013) AtALMT9 is a malate-activated vacuolar chloride channel required for stomatal opening in Arabidopsis. *Nat Commun* 4:1804.
9. Franks PJ, Buckley TN, Shope JC, Mott KA (2001) Guard Cell Volume and Pressure Measured Concurrently by Confocal Microscopy and the Cell Pressure Probe. *Plant Physiology* 125:1577-1584.
10. Shope JC, DeWald DB, Mott KA (2003) Changes in Surface Area of Intact Guard Cells Are Correlated with Membrane Internalization. *Plant Physiology* 133:1314-1321.
11. Tanaka Y, *et al.* (2007) Intra-vacuolar reserves of membranes during stomatal closure: the possible role of guard cell vacuoles estimated by 3-D reconstruction. *Plant and Cell Physiology* 48:1159-1169.
12. Bak G, *et al.* (2013) Rapid Structural Changes and Acidification of Guard Cell Vacuoles during Stomatal Closure Require Phosphatidylinositol 3,5-Bisphosphate. *Plant Cell* 25:2202-2216.
13. Gao XQ, *et al.* (2005) The dynamic changes of tonoplasts in guard cells are important for stomatal movement in Vicia faba. *Plant Physiology* 139:1207-1216.
14. Li LJ, Ren F, Gao XQ, Wei PC, Wang XC (2013) The reorganization of actin filaments is required for vacuolar fusion of guard cells during stomatal opening in Arabidopsis. *Plant Cell Environ* 36:484-497.
15. Isayenkov S, Isner JC, Maathuis FJ (2010) Vacuolar ion channels: Roles in plant nutrition and signalling. *Febs Letters* 584:1982-1988.
16. Gobert A, Isayenkov S, Voelker C, Czempinski K, Maathuis FJ (2007) The two-pore channel TPK1 gene encodes the vacuolar K+ conductance and plays a role in K+ homeostasis. *Proceedings of the National Academy of Sciences of the United States of America* 104:10726-10731.
17. Barragan V, *et al.* (2012) Ion Exchangers NHX1 and NHX2 Mediate Active Potassium Uptake into Vacuoles to Regulate Cell Turgor and Stomatal Function in Arabidopsis. *Plant Cell* 24:1127-1142.
18. Shi HZ, Zhu JK (2002) Regulation of expression of the vacuolar Na+/H+ antiporter gene AtNHX1 by salt stress and abscisic acid. *Plant Molecular Biology* 50:543-550.
19. Talbott LD, *et al.* (2006) Reversal by green light of blue light-stimulated stomatal opening in intact, attached leaves of Arabidopsis operates only in the potassium-dependent, morning phase of movement. *Plant and Cell Physiology* 47:332-339.
20. Leidi EO, *et al.* (2010) The AtNHX1 exchanger mediates potassium compartmentation in vacuoles of transgenic tomato. *The Plant Journal* 61:495-506.
21. Wang Y, Wu WH (2010) Plant sensing and signaling in response to K+-deficiency. *Molecular Plant* 3:280-287.
22. Merlot S, *et al.* (2002) Use of infrared thermal imaging to isolate Arabidopsis mutants defective in stomatal regulation. *The Plant Journal* 30:601-609.
23. Webb AA (2003) The physiology of circadian rhythms in plants. *New Phytologist* 160:281-303.
24. Dodd AN, *et al.* (2007) The Arabidopsis circadian clock incorporates a cADPR-based feedback loop. *Science* 318:1789-1792.
25. Covington MF, Harmer SL (2007) The circadian clock regulates auxin signaling and responses in Arabidopsis. *PLoS Biol* 5:e222.
26. Pei ZM, *et al.* (2000) Calcium channels activated by hydrogen peroxide mediate abscisic acid signalling in guard cells. *Nature* 406:731-734.
27. Suhita D, Raghavendra AS, Kwak JM, Vavasseur A (2004) Cytoplasmic alkalization precedes reactive oxygen species production during methyl jasmonate- and abscisic acid-induced stomatal closure. *Plant Physiology* 134:1536-1545.
28. Islam MM, *et al.* (2010) Roles of AtTPC1, vacuolar two pore channel 1, in Arabidopsis stomatal closure. *Plant and Cell Physiology* 51:302-311.
29. Bassil E, *et al.* (2011) The Arabidopsis Na+/H+ antiporters NHX1 and NHX2 control vacuolar pH and K+ homeostasis to regulate growth, flower development, and reproduction. *Plant Cell* 23:3482-3497.
30. Humble GD, Hsiao TC (1969) Specific requirement of potassium for light-activated opening of stomata in epidermal strips. *Plant Physiology* 44:230-234.
31. Robinson MF, Very AA, Sanders D, Mansfield T (1997) How can stomata contribute to salt tolerance? *Annals of Botany* 80:387-393.
32. Ivashikina N, Hedrich R (2005) K+ currents through SV-type vacuolar channels are sensitive to elevated luminal sodium levels. *Plant Journal* 41:606-614.
33. Lebaudy A, *et al.* (2008) Plant adaptation to fluctuating environment and biomass production are strongly dependent on guard cell potassium channels. *Proceedings of the National Academy of Sciences of the United States of America* 105:5271-5276.
34. Roelfsema MR, Hedrich R (2005) In the light of stomatal opening: new insights into 'the Watergate'. *New Phytologist* 167:665-691.
35. Klein M, Cheng G, Chung M, Tallman G (1996) Effects of turgor potentials of epidermal cells neighbouring guard cells on stomatal opening in detached leaf epidermis and intact leaflets of Vicia faba L. (faba bean). *Plant, Cell & Environment* 19:1399-1407.
36. Ache P, *et al.* (2010) Stomatal action directly feeds back on leaf turgor: new insights into the regulation of the plant water status from non-invasive pressure probe measurements. *The Plant Journal* 62:1072-1082.
37. Weinert S, *et al.* (2010) Lysosomal pathology and osteopetrosis upon loss of H+-driven lysosomal Cl- accumulation. *Science* 328:1401-1403.
38. Cole L, Hyde G, Ashford A (1997) Uptake and compartmentalisation of fluorescent probes by Pisolithus tinctorius hyphae: evidence for an anion transport mechanism at the tonoplast but not for fluid-phase endocytosis. *Protoplasma* 199:18-29.
39. Talbott LD, Zeiger E (1996) Central Roles for Potassium and Sucrose in Guard-Cell Osmoregulation. *Plant Physiology* 111:1051-1057.
40. Talbott LD, Zeiger E (1998) The role of sucrose in guard cell osmoregulation. *Journal of*

Experimental Botany 49:329-337.
41. MacRobbie EA (2006) Osmotic effects on vacuolar ion release in guard cells. *Proceedings of the National Academy of Sciences of the United States of America* 103:1135-1140.
42. Walker DJ, Leigh RA, Miller AJ (1996) Potassium homeostasis in vacuolate plant cells. *Proceedings of the National Academy of Sciences of the United States of America* 93:10510-10514.
43. Leigh RA (2001) Potassium homeostasis and membrane transport. *Journal of Plant Nutrition and Soil Science* 164:193-198.
44. Chen ZH, *et al.* (2012) Systems dynamic modeling of the stomatal guard cell predicts emergent behaviors in transport, signaling, and volume control. *Plant Physiol* 159:1235-1251.
45. Wang Y, *et al.* (2012) Systems dynamic modeling of a guard cell Cl- channel mutant uncovers an emergent homeostatic network regulating stomatal transpiration. *Plant Physiol* 160:1956-1967.
46. Laanemets K, *et al.* (2013) Mutations in the SLAC1 anion channel slow stomatal opening and severely reduce K+ uptake channel activity via enhanced cytosolic [Ca2+] and increased Ca2+ sensitivity of K+ uptake channels. *New Phytol* 197:88-98.
47. Jossier M, *et al.* (2010) The Arabidopsis vacuolar anion transporter, AtCLCc, is involved in the regulation of stomatal movements and contributes to salt tolerance. *Plant Journal* 64:563-576.
48. Martinoia E, Meyer S, De Angeli A, Nagy R (2012) Vacuolar transporters in their physiological context. *Annual Review Plant Biology* 63:183-213.
49. Qiu QS, Fratti RA (2010) The Na+/H+ exchanger Nhx1p regulates the initiation of Saccharomyces cerevisiae vacuole fusion. *Journal of cell science* 123:3266-3275.
50. Hedrich R, Marten I (2011) TPC1-SV channels gain shape. *Molecular Plant* 4:428-441.
51. Cormack BP, Valdivia RH, Falkow S (1996) FACS-optimized mutants of the green fluorescent protein (GFP). *Gene* 173:33-38.
52. Peiter E, *et al.* (2005) The vacuolar Ca2+-activated channel TPC1 regulates germination and stomatal movement. *Nature* 434:404-408.
53. Schmid B, Schindelin J, Cardona A, Longair M, Heisenberg M (2010) A high-level 3D visualization API for Java and ImageJ. *BMC Bioinformatics* 11:274.
54. Viotti C, *et al.* (2013) The Endoplasmic Reticulum Is the Main Membrane Source for Biogenesis of the Lytic Vacuole in Arabidopsis. *Plant Cell*.

SUPPORTING INFORMATION

This section contains 7 Supplementary Figures and 1 Table, with the corresponding Supplementary Methods.

TEXT S1

Elemental X-ray analysis

To estimate the size of the vacuolar K^+ pool in in guard cells, freeze-fractured leaves of L14 plants grown in LAK medium with 1 mM K^+ were analyzed in a Scanning Electron Microscope fitted with Energy Dispersive X-Ray Spectroscopy (SEM-EDX) as described by (1). Potassium contents in plant tissues were determined by measuring fresh- and dry-weight after drying samples at 70 ºC for 48 h in a forced-air oven to obtain water contents (g water per g dry weight). Potassium was extracted by autoclaving finely ground material and then measured by atomic absorption spectrophotometry (Perkin-Elmer 1100B, Norwalk, CT, USA).

Gene contructs and transgenic lines

The C-terminus of the NHX2 and the N-terminus of the GFP polypeptides were modified by PCR using oligonucleotides NHX2-*Ngo*MIV: 5'-ACCTCCGCCGGCAGGTTTACTAAGATC-3' and GFP-*Ngo*MIV: 5'-GCCGGCGGAGGTGTGAGCAAGGGCGAGG-3'. *Ngo*MIV digestion of amplified sequences and subsequent ligation generated an in-frame fusion of GFP to the C-terminus of NHX2 that was cloned into the *Eco*RV site of the pBluescript polylinker. Next, the NHX2:GFP construct was moved as a 2998 bp *Xho*I-*Bam*HI fragment to the plant transformation plasmid pBI321 (2). The C-terminus of TIP1;1 and the N-terminus of the GFP polypeptides were modified by PCR using oligonucleotides TIP-Not: 5′-CCACCGCGGCCGCCGTAGTCTGTGGTTGGGAG-3' and GFP-Not: 5′-GCTGGCGGCCGCGGTGGTGTGAGCAAGGGCGAGGAGCTG-3'. *Not*I digestion of amplified sequences and ligation generated an in-frame fusion of GFP to the C-terminus of TIP1;1. Plasmid pBI321Kan-TIP:GFP was constructed by cloning the TIP1;1:GFP translational fusion into pBI321 as a 1497 bp *Xho*I-*Bam*HI fragment. Plasmids pBI321Kan-TIP:GFP and pBI321-NHX2:GFP were used to transform Col-0 wild-type plants. Single-copy homozygous transformants in Col-0 were selected after three cycles of self-crossing from a T_1 population that exhibited a 3:1 segregation of the Kan^R marker. Null *nhx1 nhx2* mutant plants were both recalcitrant to transformation and resistant to kanamycin due to the mutagenic T-DNA insertions (1). Therefore, a hemizygote of genotype *nhx1-2/nhx1-2 NHX2/nhx2-1* was transformed with the pBI321Hyg-TIP:GFP plasmid carrying the hygromycin resistance marker. This plasmid was obtained by replacing the *NOS-NPTII-NOS* expression cassette of pBI321Kan-TIP:GFP with a *NOS-HptII-NOS* cassette using the *Cla*I/*Pme*I sites. Hygromycin-resistant segregants carrying

the TIP1;1:GFP construct were screened by diagnostic PCR with allele-specific primers designed to amplify wild-type or mutant *NHX2* alleles to identify homozygous *nhx1-2 nhx2-1* null mutants. *Agrobacterium tumefaciens*-mediated transformation was according to (3) and transgenic plants were selected on half-strength MS medium containing hygromycin (20 mg L^{-1}) or kanamycin (50 mg L^{-1}).

Semiquantitative RT-PCR

To study the transcriptional regulation of *NHX1* and *NHX2* genes along a day/night cycle, leaves of 6-week old Col-0 plants were harvested and frozen in liquid nitrogen at different time points: light onset, 2h and 4h of light, dusk, and 4h in the dark. Total RNA from leaves was extracted using TRIsure™ reagent according to the manufacturer's instructions (Bioline, London, UK). Reverse transcription was performed on 1 µg of total RNA using the QuantiTect® Reverse Transcription Kit following the manufacturer's instruction (Qiagen, Hilden, Germany). PCR was performed with specific primers for *NHX1* (forward 5'-GTATCTATGGCTCTTGCATACAAC-3' and reverse 5'-ATCAAAGCTTTTCTTCCACGTTACCC-3'), *NHX2* (forward 5'-CAGGGCACACAGAATTGCGCGGGAATG-3' and reverse 5'-GTCACCATAAGAGGGAAGAGCAAG-3') and *β-Tubulin-4 (TB4)* (forward 5'-CAGTGTCTGTGATATTGCACC-3' and reverse 5'- GACAACATCTTAAGTCTCGTA-3'). Densiometry analysis of the bands in ethidium bromide-stained agarose gels was performed with the software Quantity One® (Bio-Rad). The ratio between the *NHX1/2* and *TB4* transcripts was calculated to normalize for initial variations in sample concentration. Mean and standard error of the three replicas were calculated after normalization to *TB4*.

Real-Time RT-PCR

Total RNA was extracted from Arabidopsis leaves using the RNeasy plant mini kit (Qiagen, Hilden, Germany) and reverse transcription was performed on 1 µg of total RNA using the QuantiTect® Reverse Transcription Kit following the manufacturer's instruction (Qiagen, Hilden, Germany). Real-time PCR was performed using iTaq Universal SYBR Green Supermix (Bio-Rad), and the signals were detected on an iCYCLER (Bio-Rad). The cycling profile consisted of 95°C for 10 min followed by 45 cycles of 95°C for 15 s and 60°C for 1 min. A melting curve from 60 to 90°C was run following the PCR cycling to confirm the specificity of the primers. The expression levels of *NHX1* and *NHX2* genes were normalized to the constitutive *UBQ10* gene *(At4g05320)* by subtracting the cycle threshold (CT) value of *UBQ10* from the CT value of the gene (ΔCT). The fold change was calculated as $2^{-(\Delta CT\ mutant\ -\ \Delta CT\ wild\ type)}$. The results shown are from three technical replicates of three independent RNA samples obtained from three different plants per genotype. Samples were obtained at two different time points of the day/night cycle from the same plants used for determing stomatal conductance of *nhx1-2* and *nhx2-1* single

mutants. Primers user for qRT-PCR were: *NHX1qRT* 5'- GAGGTCGTGGCTTTGTACCC-3', *NHX1*rtR 5'- ATCAAAGCTTTTCTTCCACGTTACCC-3', *NHX2qRT* 5'- GACTGAGAGAAGCAGCCATGA-3', *NHX2*rtR 5'- GTCACCATAAGAGGGAAGAGCAAG-3', *UBQ10F* 5'- GGCCTTGTATAATCCCTGATGAATAAG-3', *UBQ10R* 5'- AAAGAGATAACAGGAACGGAAACATAGT-3'

REFERENCES

1. Barragan V*, et al.* (2012) Ion Exchangers NHX1 and NHX2 Mediate Active Potassium Uptake into Vacuoles to Regulate Cell Turgor and Stomatal Function in Arabidopsis. *Plant Cell* 24:1127-1142.
2. Martinez-Atienza J*, et al.* (2007) Conservation of the salt overly sensitive pathway in rice. *Plant Physiology* 143:1001-1012.
3. Clough SJ, Bent AF (1998) Floral dip: a simplified method for Agrobacterium-mediated transformation of Arabidopsis thaliana. *Plant Journal* 16:735-743.

LEGENDS TO SUPPORTING FIGURES

Figure S1. Altered morphology of stomata and leaf epidermis in the *nhx1 nhx2* mutant

(A) SEM images of leaves from Arabidopsis Col-0 and the KO line grown in hydroponic culture with LAK medium at 1 mM KCl. Upper panels, appareance of the lower epidermis, scale bars: 200 µm; note the irregular distribution of cell sizes in the mutant. Middle panels, groups of stomata in the abaxial epidermis, scale bars: 50 µm; note the deflated appareance of the stomata show in the inset. Lower row panels, close up images of stomata, scale bars: 20 µm. **(B)** Epidermal cell density (left panel), stomatal density (middle) and stomatal index (right) calculated from dental resin impression images. Data represent means and SE from of least 42 images per line. Asterisks indicate statistically significant differences at $p<0.05$ in pairwise comparison by the Tukey's HSD test.

Figure S2. Stomatal conductance and transcript abundance in single *nhx1* and *nhx2* mutants

(A) Stomatal conductance measurements in leaves of Col-0 and single mutant lines *nhx1-2* and *nhx2-1* at different time points of the day/night cycle. Dawn and dusk samples were collected 15 minutes before light was switched on and off, respectively. Data represent mean and SE of 3 plants per line. **(B)** Quantitative RT-PCR analysis of *NHX1* and *NHX2* mRNA expression levels in whole leaves at different time points of the day/night cycle. Samples were collected from plants shown in (A), with 3 technical replicas each (n = 9), at time points 2 h after the onset of light and after 4 hours in darkness. The transcript levels were normalized to the constitutive *UBQ10* gene. Data shown are the means ± SE and represent the transcript levels of *NHX1* in the *nhx2-1* mutant plants and of *NHX2* in *nhx1-2* plants, relative to the transcript levels obtained for the wild-type Col-0 in the dark.

Figure S3. Plant growth and K^+ content under water stress.

(A) Col-0, L14 and KO plants growing in individual pots, before treatment and after 2, 4, 12 and 25 days after drought stress. **(B)** Shoot biomass and K^+ content on a dry matter basis of wild type plants (Col-0), the *nhx1-1 nhx2-1* mutant line (L14), and the *nhx1-2 nhx2-1* null mutant line (KO) grown in individual soil pots for 5 days without watering. The data correspond to plant samples (3-4 plants per line) of the experiment shown in (A). **(C)** Drought tolerance test of wild type Col-0 (W), L14 (L) and KO plants (K) growing in the same soil tray. Plants were grown for 6 weeks in short day conditions (upper panel) and then subjected to drought stress by ceasing watering for 12 days (lower panel).

Figure S4. Stomatal response to calcium and sodium salts.

(A) Calcium-induced stomata closure. Data represent the mean and SE of the absolute values of aperture of at least 150 stomata per line and treatment. Letters indicate statistically significant differences between treatments for each line at $p<0.001$ in pairwise comparison by the Tukey's

HSD test. **(B)** Stomatal opening in the presence of sodium. Light-induced stomatal opening bioassays with wild-type Col-0 plants were conducted in buffers containing 10 mM KCl or NaCl at 30, 50 and 75 mM. Data represent the mean and SE of the stomatal apertures of at least 40 stomata per treatment. Asterisks indicate statistically significant differences relative to the K^+ treatment at $p<0.001$ in pairwise comparison by the Tukey's HSD test. **(C)** Reversal of sodium-driven stomatal opening by ABA. Light-induced stomatal opening in 50 mM NaCl for 4 h was followed by treatment with 1 µM ABA for one additional hour. Data represent the mean and SE of the stomatal apertures of at least 50 stomata per treatment.

Figure S5. Time-lapse of vacuolar dynamics in leaf discs during stomatal closure.
Vacuolar structure of Col-0 and KO guard cells visualized in leaf discs with TIP1;1:GFP at different time points after 10 µM ABA treatment. Left and right panels show bright field and GFP images of TIP1;1:GFP, respectively. Scale bar: 5 µm.

Figure S6. Time-lapse of vacuolar dynamics in leaf discs during stomatal opening.
Vacuolar structures in guard cells of Col-0 and KO plants visualized with TIP1;1:GFP at different time points after 3 µM fusicoccin treatment. Left and right panels show bright field and fluorescence images of TIP1;1:GFP, respectively. Scale bar: 5 µm.

Figure S7. Vacuolar compartmentation of the dye and ratiometric pH calibration curve.
(A) Vacuolar lumen of open (upper panel) and closed (lower panel) wild-type stomata loaded with the pH-sensitive dye Oregon Green. Left and right panels show bright field and 488-nm-excited images, respectively. Scale bar: 5 µm. **(B)** The mean ratios obtained from dividing the pixel density of 488-nm-excited images by the pixel density of 458-nm-excited images from guard cell vacuoles loaded with the pH-sensitive dye Oregon Green were plotted against the pH of the equilibration buffer. Data represent means and SE from at least 20 stomata per treatment.

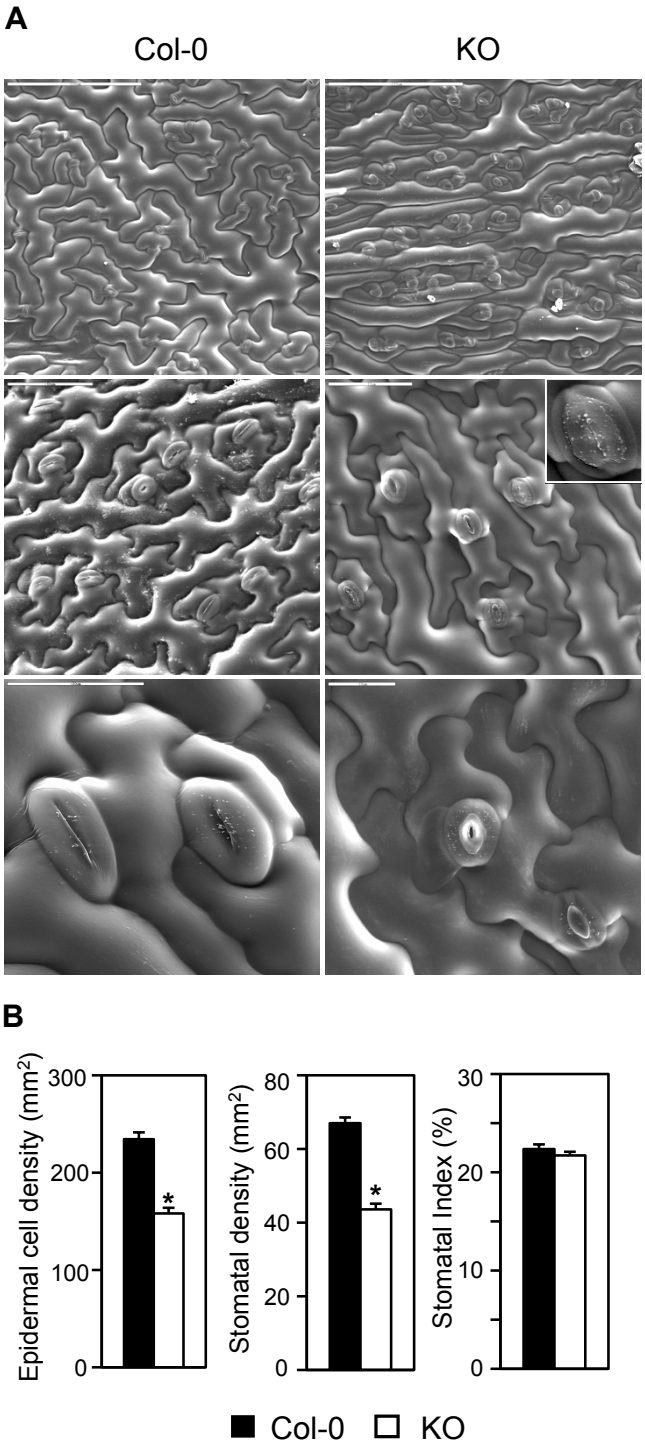
A
Col-0
KO
B
Epidermal cell density (mm2)
300
200
100
0
*
Stomatal density (mm2)
80
60
40
20
0
*
Stomatal Index (%)
30
20
10
0
Col-0
KO

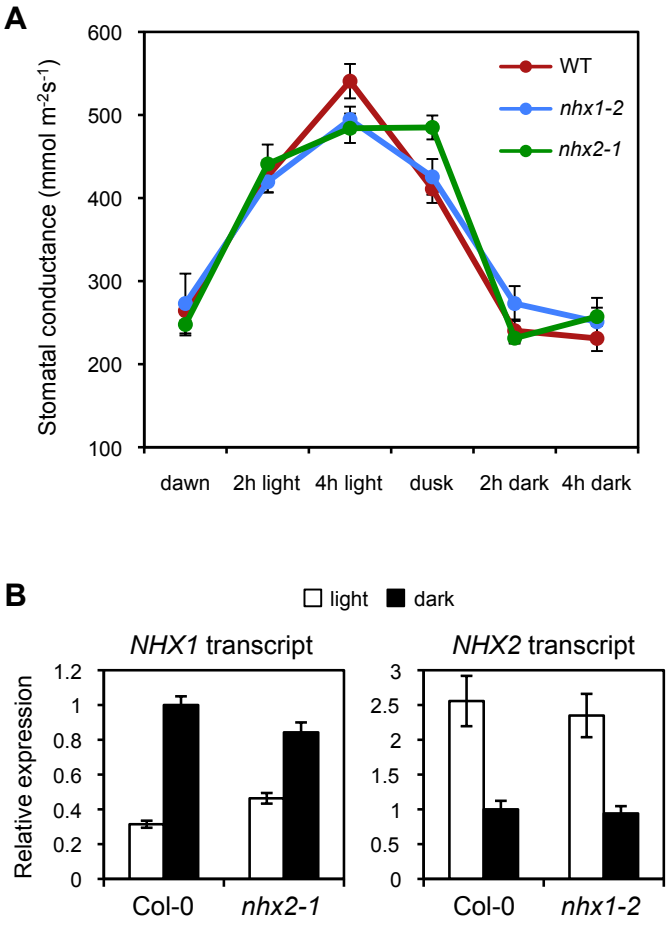
A
600
500
400
300
200
100
Stomatal conductance (mmol m-2s-1)
WT
nhx1-2
nhx2-1
dawn
2h light
4h light
dusk
2h dark
4h dark
B
light
dark
NHX1 transcript
NHX2 transcript
Relative expression
1.2
1
0.8
0.6
0.4
0.2
0
3
2.5
2
1.5
1
0.5
0
Col-0
nhx2-1
Col-0
nhx1-2

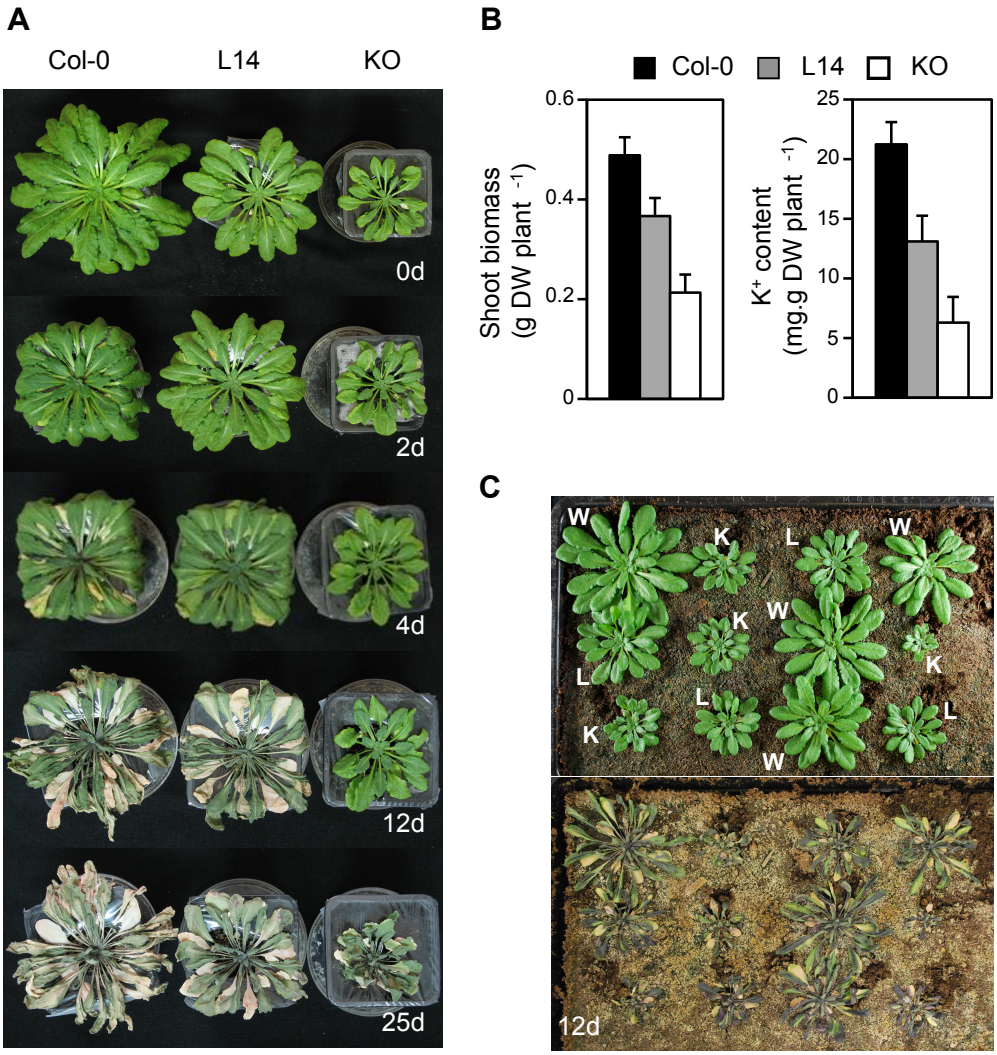
A
Col-0
L14
KO
0d
2d
4d
12d
25d
B
Col-0
L14
KO
Shoot biomass
(g DW plant -1)
0.6
0.4
0.2
0
K+ content
(mg.g DW plant -1)
25
20
15
10
5
0
C
W
K
L
12d

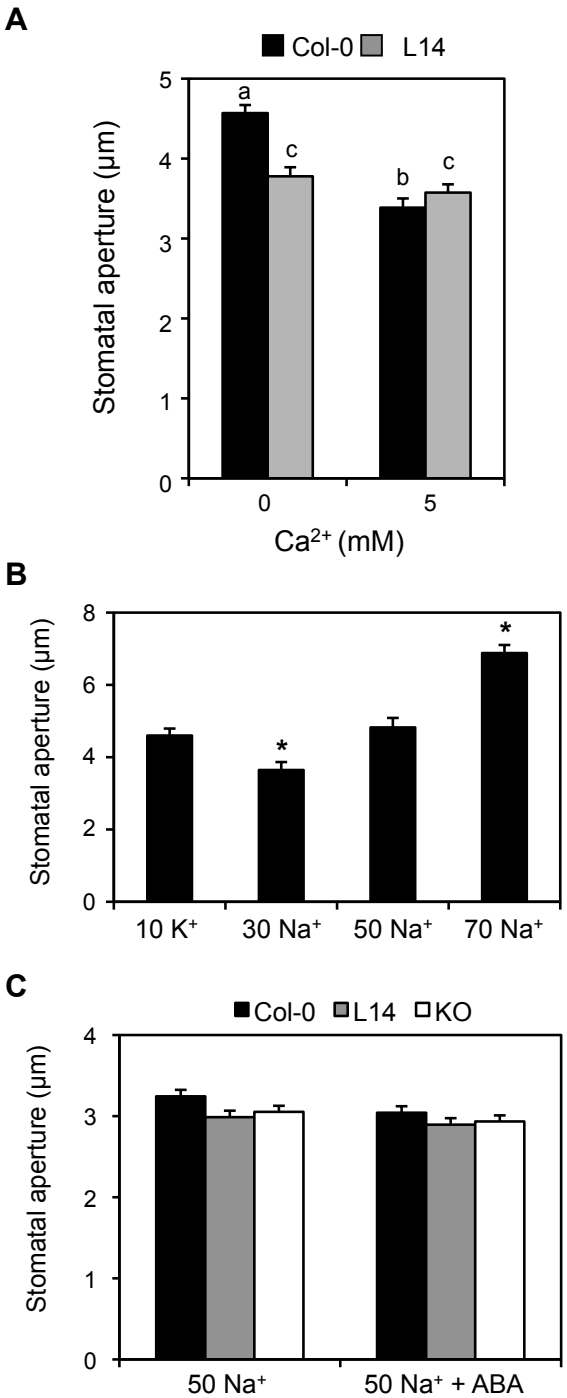
A
Col-0
L14
Stomatal aperture (µm)
a
c
b
c
0
1
2
3
4
5
0
5
Ca2+ (mM)
B
Stomatal aperture (µm)
*
*
0
2
4
6
8
10 K+
30 Na+
50 Na+
70 Na+
C
Col-0
L14
KO
Stomatal aperture (µm)
0
1
2
3
4
50 Na+
50 Na+ + ABA

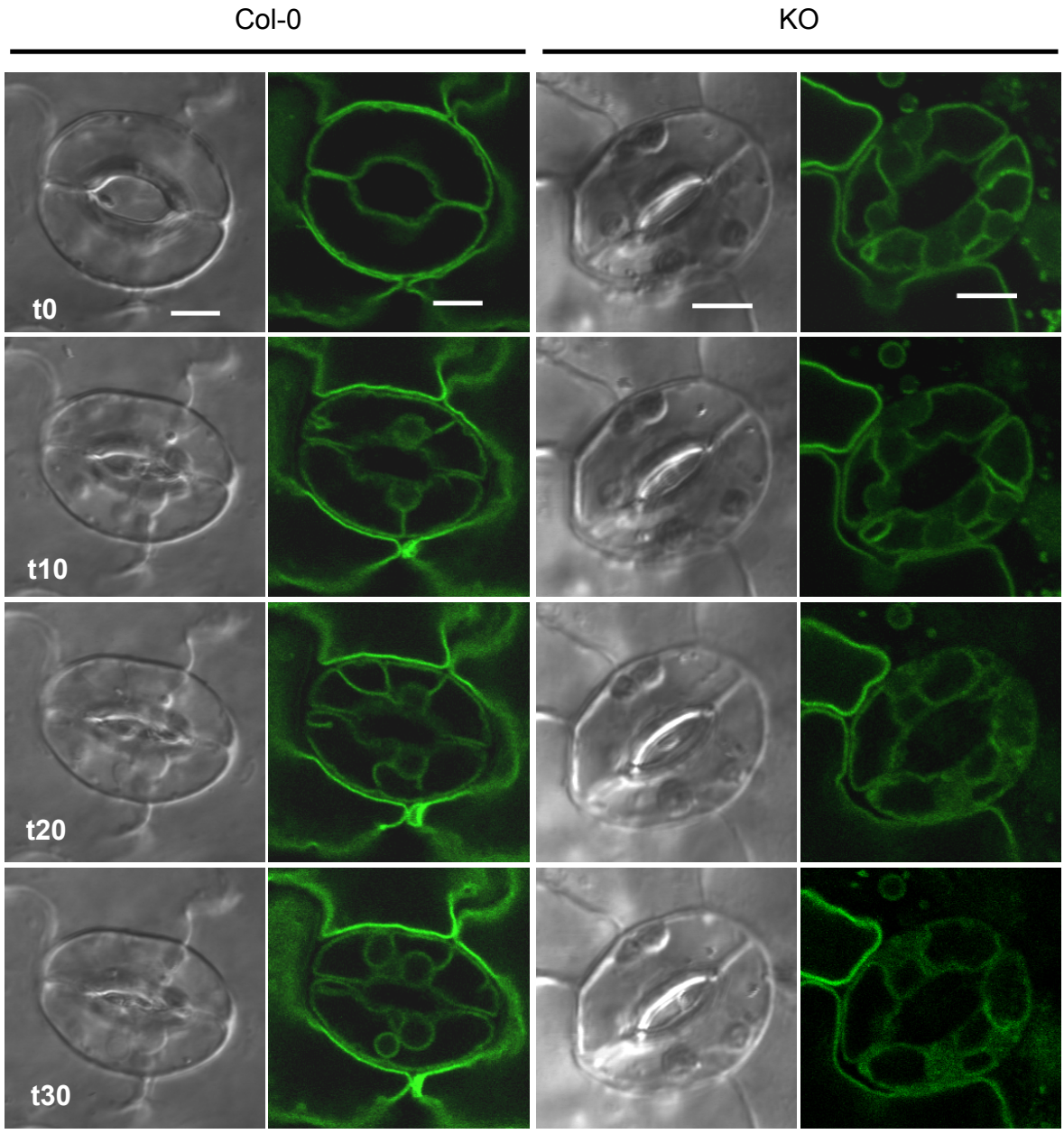
Col-0
KO
t0
t10
t20
t30

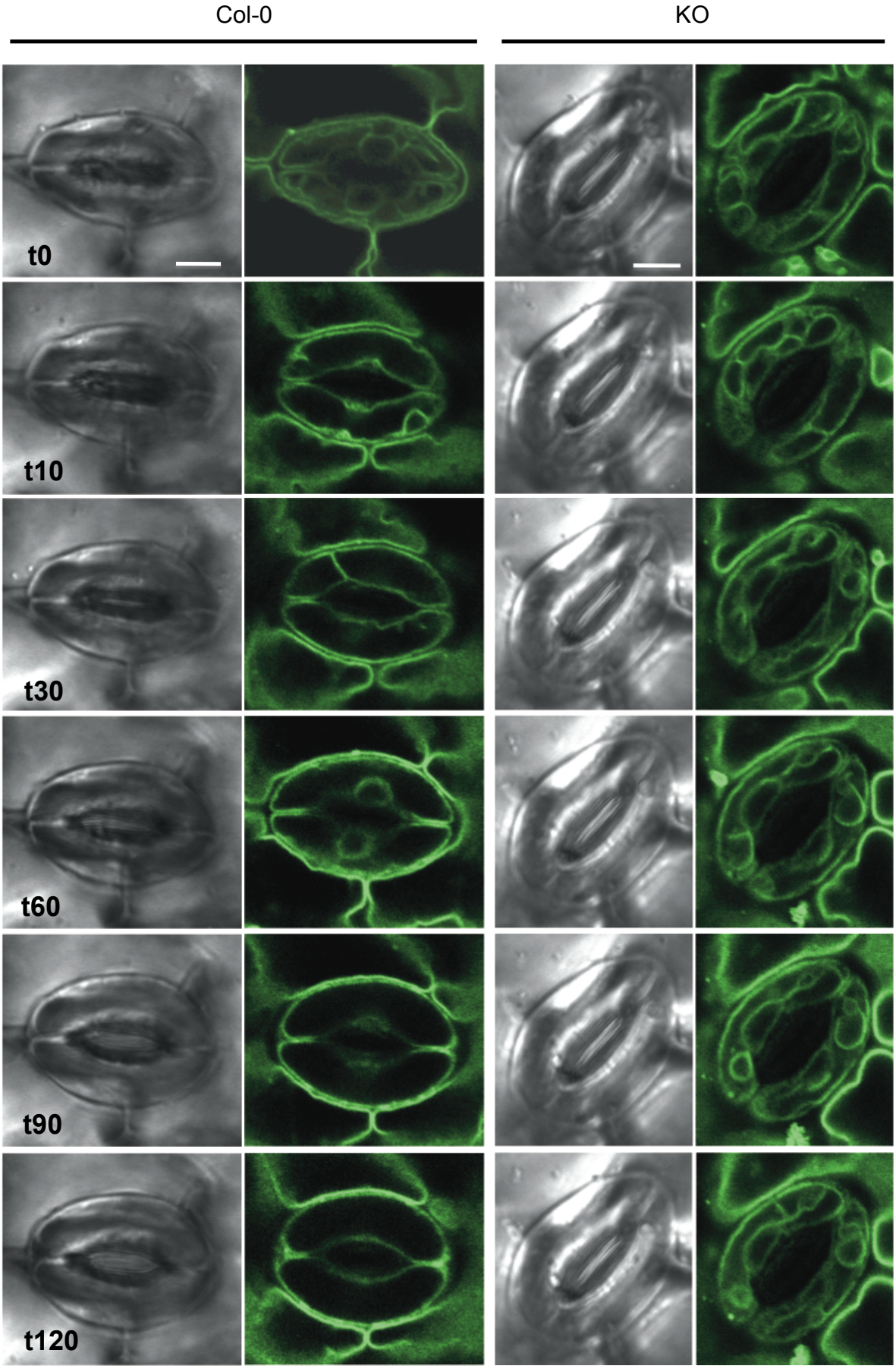
Col-0
KO
t0
t10
t30
t60
t90
t120

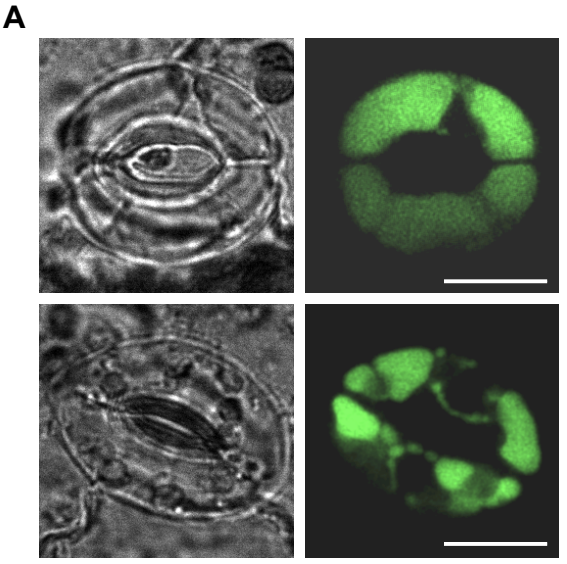
A
B
Ratio 488/458 nm
1.8
1.6
1.4
1.2
1.0
4.5
5.0
5.5
6.0
6.5
pH

SUPPLEMENTARY TABLE

Table S1. Mean temperatures determined by thermal imaging of wild-type plants and *nhx1 nhx2* mutant lines at different day and night periods. Statistical significance of differences in mean temperatures between the wild type and mutant lines was determined by the Student's *t*-test. ** $P < 0.001$, * $P < 0.05$, and ns = no significant difference.

Period (minutes)	**Line**	**Mean ± SD (ºC)**	**Paired differences Mean ± SD (ºC)**
P1 (40-170) Day	Col-0	20.822 ± 0.266	
	L14	20.880 ± 0.253	0.058 ± 0.022**
	KO	21.110 ± 0.187	0.288 ± 0.084**
P2 (300-400) Night	Col-0	20.512 ± 0.229	
	L14	20.416 ± 0.226	0.097 ± 0.042**
	KO	20.222 ± 0.171	0.290 ± 0.070**
P3 (600-700) Night	Col-0	20.522 ± 0.366	
	L14	20.429 ± 0.355	0.092 ± 0.037**
	KO	20.158 ± 0.273	0.363 ± 0.111**
P4 (800-900) Night	Col-0	20.464 ± 0.363	
	L14	20.455 ± 0.353	0.009 ± 0.036*
	KO	20.189 ± 0.272	0.276 ± 0.105**
P5 (950-1050) Night	Col-0	20.406 ± 0.165	
	L14	20.403 ± 0.170	0.002 ± 0.028ns
	KO	20.147 ± 0.126	0.259 ± 0.055**
P6 (1100-1227) Day	Col-0	20.984 ± 0.144	
	L14	21.073 ± 0.139	0.089 ± 0.019**
	KO	21.197 ± 0.129	0.213 ± 0.069**